MDPI

Article

The Importance of Geotechnical Evaluation and Shoreline Evolution in Coastal Vulnerability Index Calculations

Vasileios Boumboulis, Dionysios Apostolopoulos [ID]**, Nikolaos Depountis ***[ID] **and Konstantinos Nikolakopoulos** [ID]

Department of Geology, Division of Applied Geology and Geophysics, University of Patras, 26504 Patras, Greece; vasileios_boumpoulis@upnet.gr (V.B.); apostolopoulos.dionysios@upatras.gr (D.A.); knikolakop@upatras.gr (K.N.)
* Correspondence: ndepountis@upatras.gr

Abstract: The aim of this specific study is to present a new weighted Coastal Vulnerability Index (CVI_{WF}), with an emphasis given to the geotechnical evaluation and shoreline evolution rate measured through high-resolution remote sensing, which seem to be the most interfering variables in CVI calculations. As a pilot area for the application of the new CVI_{WF}, the Gulf of Patras in Western Greece was selected, which is suffering erosion problems due to climate change, the sea level rising and human intervention. The new CVI_{WF}, which was applied in this research, includes the following innovations: (1) the use of geotechnical characterization instead of geological–geomorphological characterization, (2) the use of high-resolution remote sensing data for the detection of shoreline evolution rate and (3) the insertion of a specific weighted geotechnical factor in the CVI_{WF} formula. The results from the application of the unweighted CVI show that percentages of 20.13%, 20.47%, 24.56%, 29.39% and 5.45% of the gulf's shoreline are under the regime of very low, low, moderate, high and very high vulnerability, respectively. On the other hand, the corresponding results from the application of the weighted CVI_{WF} show a percentage of 14.59%, 25.91%, 20.04, 36.48% and 2.98, respectively.

Keywords: Coastal Vulnerability Index (CVI); geotechnical evaluation; shoreline evolution; Geographical Information Systems (GIS); coastal erosion

1. Introduction

The coastal zone can be considered as the geographical area of interaction between marine and land area (land–sea interface), which coexists with human societies, as well as socioeconomic and human activities. The rising sea level and extreme events related to climate change are causing severe threats to coastal areas, affecting both natural and human systems worldwide [1]. One of the most common and diachronic problems in coastal zones is sea–wave erosion, named coastal erosion. In Greece, more than 20% of its total shoreline [2] is threatened by coastal erosion and rising sea levels, ranking the country fourth in terms of coastal vulnerability among the 22 coastal EU member states. In this already complicated scenario, coastal areas are also experiencing relevant pressures resulting from multiple human-induced stressors linked with coastal economic development (e.g., touristic activities and infrastructures along the shoreline) and the connected land use changes (e.g., urbanization) [3]. Due to the continuous development and the increasing population living in the coastal zone (half of EU population lives in regions within 50 km of the coast) [4], the construction of various technical works is required, such as buildings, infrastructures, roads, ports and coastal defense works. However, coastal areas are vulnerable and susceptible to coastal hazards like storm surges, tsunamis, floods, coastal erosion, sea level rise, etc. Climate change, global warming and, as a result, the sea level rise (SLR) can cause accelerated erosion, shoreline retreat in coastal zones and saltwater intrusion into groundwater aquifers [5]. In a very recent study [6], it has been indicated that most coastal countries in Europe (including Greece) are planning

for SLR with the horizon the year of 2100. For these reasons, the assessment of vulnerability to the impact of the rising sea levels and coastal hazards is an important aspect of coastal zone management and coastal protection [7].

In many countries and institutions, different risk assessment methodologies have been developed to understand the processes underpinning coastal erosion risks [8–12]. As a result, several tools and methods supporting policy and decision makers in the implementation of recommendations, and directives for coastal zone management have been developed in several countries [13–15], with one of the most important aspects being coastal vulnerability. The assessment and calculation of coastal vulnerability, focusing on coastal erosion processes, is accomplished with the following methods: (a) methods based on a specific vulnerability index, (b) methods based on a sequence of indicators, (c) methods based in geographical information system (GIS)-based decision-making systems and (d) methods based on dynamic computational models [3]. The most common used method is the vulnerability index, which is considered as a consistent, easy and fast way to calculate the vulnerability of coasts. This approach combines the "sensitivity" of the coastal system to changes (shoreline differentiation due to rising sea levels) with its natural ability to adapt to changing environmental conditions [16]. The most used and accepted method of calculating coastal vulnerability is the Coastal Vulnerability Index (CVI). The CVI was developed by Gornitz [16,17] and modified by Thieler and Hammer-Klose [18,19] for the evaluation of vulnerability throughout the United States. The most common parameters used in the CVI methodology are (a) geology and geomorphology, (b) coastal slope, (c) shoreline change rate, (d) average tidal range, (e) change in the sea level and (f) average significant wave height.

Many researchers have used vulnerability indexes or similar modified models for the assessment of coastal vulnerability to erosion in coastal zones [20–27]. For example, Diez et al. [21] changed the variable of coastal slope with elevation and inserted local tectonics affections, while Pramanik et al. [28] used seven parameters and different conventional and remotely sensed data. Rao et al. [7] added weighted values in the calculation formulas, and Ruzic et al. [29] improved the CVI for complex geologic conditions by adding a weighted factor in the parameter of geology. De Serio et al. [30] and Zhu et al. [31] performed a multicriteria evaluation method, named the Analytical Hierarchy Process (AHP). in the Adriatic Sea, Italy and in China, respectively. Greco and Martino [32] integrated in their CVI approach the study of time-dependent vulnerability together with information on the morphology and socioeconomic features, showing that vulnerability is not static in time but evolves according to changing patterns in the climate system. Lopez et al. [33] used four different sea level rise values corresponding to the four greenhouse gas emission scenarios given by the IPCC [34] to produce CVI maps on a national scale in Spain. Rangel-Buitrago [35] developed a more complex model using forcing, susceptibility and hazard indexes. A systematic review on various Coastal Vulnerability Indexes and Mapping was given by Kantameni et al. [36], Bukvic et al. [37] and Anfuso et al. [38].

Models of the vulnerability index have also been developed with different approaches that determine the coastal vulnerability using socioeconomic variables (e.g., population density, poverty levels and land use) [39–43], while other models use socioeconomic and physical–geographical parameters, such as the SIVECA index and CERA GIS-based tool [32,44–47]. Szlafsztein and Sterr [48] introduced a Composite Vulnerability Index, allowing the combination of eight variables reflecting the natural dimension of vulnerability (e.g., coastline length, coastal protection measures and fluvial drainage) with seven other indicators reflecting the socioeconomic dimensions. Furthermore, Toressan et al. [49] introduced the methodology by integrating physical, geological and socioeconomic indicators in the CVI model and also taking into account the expected SLR and (storm surge level) flooding projections for the 2100 timeframe (i.e., climate-improved CVI).

In Greece, numerous studies have been conducted with the use of CVI or other adopted methods to assess the vulnerability to erosion. Gaki-Papanastasiou et al. [22] and Karymbalis et al. [24,25] assessed the vulnerability to an anticipated future sea-level

rise, using the Coastal Vulnerability Index (CVI) and the Coastal Sensitivity Index (CSI), respectively. Doukakis [20] added in the CVI the parameter of subsidence for Western Peloponnese, while Tragaki et al. [50] considered socioeconomic and demographic parameters for the CVI model, for the evaluation of coastal hazard vulnerability in the same area. Alexandrakis and Poulos [51] developed a new index for the evaluation of vulnerability (Beach Vulnerability Index or BVI) mainly considering hydro and sediment dynamic parameters (longshore sediment transport, riverine inputs, storm surge etc.). Finally, Alexandrakis et al. [52] combined the environmental and economic approaches along the geographical space to relate the beach erosion vulnerability with the expected land loss and the relevant values from economic activities in Crete.

Several types of methods based on remote sensing low-resolution data derived from Landsat or Sentinel images have been used in order to estimate the shoreline change rate [53–56]. Accordingly, two recent studies sited in Northwestern Peloponnese by Apostolopoulos and Nikolakopoulos [57] and Apostolopoulos et al. [58] concluded that the accuracy of the vector data derived from low-resolution data are not suitable either for shoreline forecasting or shoreline mapping. An overall review and meta-analysis of the remote-sensing data, GIS methods, materials and indices used for monitoring the coastline evolution over the last twenty years was given by Apostolopoulos and Nikolakopoulos [59].

Another important variable that proved to be very important in the determination of coastal vulnerability is shoreline evolution, otherwise known as the historical shoreline change rate, with the application of extensive remote-sensing techniques. Generally, there are two main categories of studies regarding remote-sensing monitoring: those that use free-of-charge low-resolution data and those that use high-resolution data. Over time, many studies have tried to process shoreline evolution with low-resolution satellite images, but their results always lack accuracy. Different methods have been used to overpass this drawback regarding the accuracy of the measurements and the results they provide. Pardo Pasqual et al. [53] developed a very complicated methodology in order to ameliorate the Landsat data accuracy using a high-resolution air photo mosaic by co-registering the low-resolution coastline derived from Landsat data to the respective high-resolution shoreline. In another similar study, Almonacid et al. [60] computed the average annual coastline movement of many Landsat images and yielded a mean error of -4.7 m, showing that the shorelines derived from Landsat images were placed seaward in comparison with the respective high-precision shorelines. In a recent study in Northwestern Peloponnese, Apostolopoulos and Nikolakopoulos [57] followed a statistical analysis using Digital Shoreline Analysis System (DSAS) software and concluded that low-resolution data are not suitable either for shoreline forecasting or shoreline mapping, as their accuracy are very low, and they present a divergence that ranges between 6 and 11 m. In a similar study, Apostolopoulos et al. [58] concluded that the accuracy of the vector data derived from Sentinel-2 10-m spatial resolution images ranged between 1 and 5 m using the NDVI and NDWI indices, respectively. On the other hand, the synergy of high-resolution satellite imagery and high-scale aerial photos has become a very accurate combination in order to study the coastal zone changes. In the current study the shoreline rate of change was computed based on high-resolution aerial and satellite images, improving the rate's accuracy. These datasets were processed in a GIS platform, and the statistical analysis was performed through DSAS application by computing the end point rate (EPR). The use of high-resolution data provides an improved accuracy during (CVI) analysis and gives better results in finding the respective erosion or accretion trends along the shoreline.

On the other hand, the combination of historical cartography, aerial photographs and GPS surveys has become a very accurate combination in order to study the coastal zone changes. In a recent study, Antonello Aiello et al. [61] used this combination to assess the changes of the littoral environment between 1870 and 2005 on the coastal area of the Jonian Sea in Italy. In another study, Murray Ford [62] used vertical aerial photographs along with high-resolution satellite imagery such as IKONOS (0.8-m pixel size), QuickBird (0.6-m pixel size), WordView-2 (0.5-m pixel size) and GeoEye-1 (0.5-

m pixel size) to estimate the shoreline changes in the Marshall Islands. Additionally, historical changes in the shoreline position along the Bay of Jijel, Algeria were studied by reference [63] with the combination of multi-dated aerial photographs and QuickBird (0.6-m pixel size) satellite image. Furthermore, ref. [64] a combined semi-automatic technique for coastal risk assessment and monitoring integrated ground data with Earth Observation (EO) data in Apulia Region (South Italy). Finally, reference [65] used aerial photography, Google Earth Pro and Topographic survey measurements in order to determine changes in the shoreline position in four beaches on Valparaíso Bay in Central Chile.

Taking into consideration the above methodologies, it was decided, for the purposes of the current research, to investigate more thoroughly the interference of geotechnical evaluation and shoreline change rate in the preformed CVI calculations. For this reason, the calculation of coastal vulnerability was based on the original formula of Gornitz [16,17] with the following modifications: (1) the use of geotechnical characterization instead of geological–geomorphological characterization, (2) the use of high-resolution remote-sensing data and (3) insertion of a specific geotechnical weighted factor into the CVI formula. All calculations were performed in the GIS; therefore, it finally produced a combined CVI-GIS model. The new CVI_{WF} model was also compared with an unweighted (CVI) model, and for this comparison as a pilot area, the Gulf of Patras in Western Greece was used. The reason for selecting the Gulf of Patras as a pilot area had to do with the detailed data that has been collected from recent coastal monitoring activities in the frame of the TRITON project [66]. In order to proceed with the relevant CVI_{WF} calculations, the pilot area was divided in eight coastal zones, and the geotechnical behavior of the prevailing geological formations was thoroughly investigated. The geotechnical investigation that was performed included borehole drilling, laboratory tests, Standard Penetration Tests (SPT), sediment sampling and engineering–geological mapping. This type of investigation improved the quantification of the geotechnical variable and led to a geotechnical characterization of the pilot area. Moreover, the shoreline rate of change was computed by using high-resolution aerial and satellite images, as well as the Digital Shoreline Analysis System [67] and by computing the end point rates (EPR) along the eight coastal zones of the pilot area. These rates were imported to the (CVI_{WF}) model and improved its accuracy. The final purpose of this work was mainly to highlight the importance of geotechnical evaluation in Coastal Vulnerability Index calculations, along with shoreline evolution.

2. Study Area

The Gulf of Patras is in Western Greece, Northwest Peloponnese and extends from the Rio-Antirio Bridge in the eastern part to the Cape of Araxos in the western part (Figure 1). The total length of the southern shoreline of the gulf is around 45 km, with the maximum depth of water at 130 m. The Gulf of Patras is a Plio-Quaternary graben [68]. In the west it is connected with the Ionian Sea and, in the east, with the Gulf of Corinth. The main rivers discharging into the gulf are the Acheloos River and the smaller Evinos and Peiros rivers. The evolution of the gulf in the Quaternary occurs because of the interactions between the tectonic subsidence (rates at 3–5 mm/year at the central graben), global sea level rise and river sediment supply [69].

One of the most significant hazards that threatens the area of study is coastal erosion, and according to the Hellenic legislative framework, the Gulf of Patras has been characterized as a water body at risk. Due to the above description, it is easily understandable that the assessment of vulnerability to erosion is very important for this particular area, because it will assist local authorities with important information for its future protection against erosion.
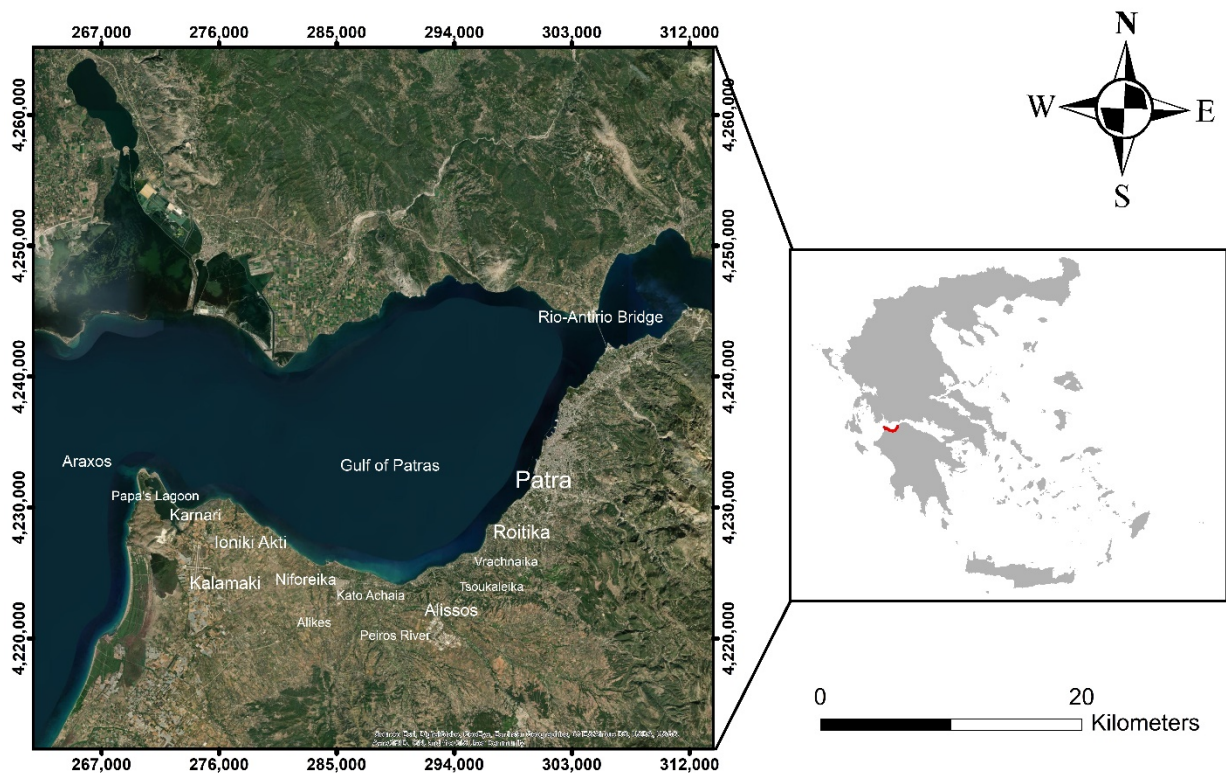
Figure 1. Map of the study area (use of the Hellenic Geodetic Reference System, 1987).

For the assessment of vulnerability, the shoreline of the Gulf of Patras was divided into eight (8) zones and each zone in equal segments of 50 m (Figure 2).
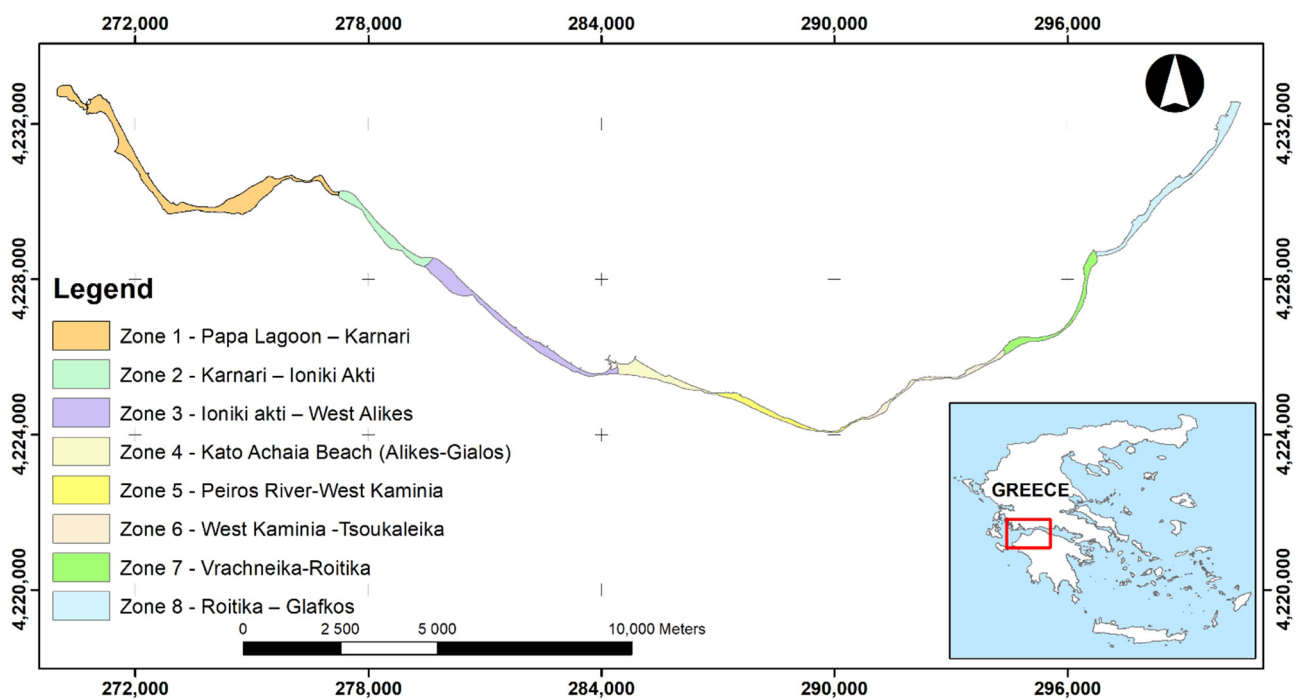

Figure 2. Map of the study area separated in eight zones (use of the Hellenic Geodetic Reference System, 1987).

3. Materials and Methods

The main features of the presented (CVI_{WF}) model are: (1) the use of geotechnical data in order to characterize the coastal formations as geotechnical units, (2) the significant mean wave height with a return period of 10 years, (3) the coastal slope, which has been calculated by using a Digital Elevation Model (DEM) (2X2 m), (4) the shoreline evolution by computing the relevant end point rates (EPR), (5) the average tidal range and (6) the sea level rise (SLR).

The calculations of the CVI were performed with two different methods: (1) with the use of the formula proposed by Gornitz [16] by computing the CVI as the square root of the product of the variables divided by their total number (*n*) and (2) with the use of the new CVI_{WF} by adding a weighted factor in the geotechnical variable, which seems to be the most representative of the resistance to erosion. The calculation of the new (CVI_{WF}) model performed with the use of data that was derived from a marine equipment that was installed in the pilot area for the purposes of the TRITON project [66]. The data acquired from the TRITON project was (a) the significant wave height and (b) the tidal range measurements. The data were derived from a tide gauge system and a wave buoy that were installed in the frame of the TRITON project. The significant wave height also was acquired by performing a numerical simulation of wave propagation for wind speed with a return period of 10 years for each wind direction, using the MIKE 21, DHI software, which was also performed in the frame of the TRITON project.

3.1. Geotechnical Characterization

The most common variables used for the description of resistance to erosion are coastal geology and geomorphology. During this research, this variable was replaced with the geotechnical characterization parameter. For this purpose, a thorough geotechnical investigation was carried out in the research area, including the drilling of forty (40) boreholes, laboratory and in-situ geotechnical tests (SPT), a numerous coastal sediment sampling and field engineering–geological mapping. An SPT in-situ geotechnical test is widely used for a soil strength characterization. The calculation of SPT can be described as the number of blows required for each 15-cm penetration of the sampler into the soil, until it penetrates 45 cm. Finally, the result of this test is the number of blows required for the penetration of the last 30 (15+15) cm and is indicated as N or N_{SPT} blow numbers [70].

The use of geotechnical data improves the quantification of the coastal resistance to the erosion parameter and is more reliable and representative, since it categorizes the total area according to the geotechnical behavior of the prevailing coastal formations. In Table 1 are presented some of the most representative geotechnical data that were used for the geotechnical characterization of the eight (8) zones of the pilot area. This method led to a new categorization depending on the geotechnical behaviors of coastal formations, which were ranked as "very low", "low", "moderate", "high" and "very high" vulnerability.

Table 1. Geotechnical characterization of the eight (8) zones existing in the Pilot area (N_{SPT}: Number of SPT blow counts and D_{50}: average grain diameter).

Zone	Name of Zone	N_{SPT}	D_{50} (mm)	Geotechnical Characterization/Units
1	Papa Lagoon—Karnari	>18	1.38	Sand with small percentage of gravels (SP, SM-SP)
2	Karnari—Ioniki Akti	>28	2.09	Medium dense sand with gravels (SP, GP) and poorly graded sand with gravels and silt (SP-SM, SP)
3	Ioniki akti—West Alikes	12	1.39–2.03	Medium dense silty sand with gravels (SP-SM) and moderately dense silty sand with few gravels (SP-SM)
4	Kato Achaia Beach (Alikes—Gialos)	13	1.10	Medium dense poorly graded sand (SP-SM) and loose to moderately dense sand with gravels (GW-GM)
5	Peiros River—West Kaminia	12–42	3.97	Medium dense sand with gravels (GM, GW-GM) and silty sand with gravels (SW-SM)
6	West Kaminia—Tsoukaleika	12	1.72	Dense sand with gravels and cobbles (GP) and poorly graded sand (SP)
7	Vrachneika—Roitika	12–49	2.07–2.66	Well graded sand with gravels (SW-SM) and poorly graded sand (SP). Sand with gravels and silt (GP-GM) and dense silty sand with gravels (GW-GM, GP-GM)
8	Roitika—Glafkos	>12		Medium dense sand with gravels and silt (GP-GM)

3.2. Significant Mean Wave Height

The main variable that affects and forces the sediment to move and transport (long-shore and cross-shore sediment transports) and causes erosion is the wave energy. High waves have bigger energy compared with low waves and, as a result, cause erosion with a higher rate. A combination of wave height, sea level rise and tidal range form the main hydrodynamic forces that cause coastal erosion and, especially, the wave height has very a high impact on coastal erosion and calculation of vulnerability. Wave height values for the coastal zone of the Gulf of Patras calculated with a numerical simulation of wave propagation for wind speed with a return period of 10 years for each wind direction using the MIKE 21, DHI software.

3.3. Coastal Slope

A shoreline with a high coastal slope is not vulnerable to SLR and shoreline retreat. However, in a flat coast (small coastal slope), a possible inundation has significant consequences, such as shoreline retreat, since a possible SLR will cause a big inundation of the sea inside the land and cover large areas. Ruzic et al. [29] inverted this rating based on the conception that high coastal slopes cause rockfalls and extreme erosion in the shoreline. The parameter of the coastal slope, during this research, was determined through a Digital Elevation Model (DEM) (2X2 m) acquired through the National Greek Cadastre and Mapping Agency and ranked with "low" vulnerability on steep coasts and "high" vulnerability on gentle coasts.

3.4. Shoreline Evolution

The shoreline evolution or change rate is an important parameter that indicates the accretion/erosion pattern in an area. The computation of a historical trend and monitoring of shoreline evolution in the pilot area was performed by using remote-sensing data processing for a 10-year period (from 2008 to 2018). High-resolution satellite data and orthomosaics were used to monitor the coastline's changes in the littoral area. In the current study, official datasets of orthomosaics for the years of 2008 and 2016 were acquired through the National Greek Cadastre and Mapping Agency with a spatial resolution of 0.5 m, which are the most accurate datasets for the Greek territory. Moreover, Worldview-2 high-resolution imagery (0.5-m spatial resolution) of the year 2018 was orthorectified and

used to extract the shoreline for that year. All remote-sensing data used for the current research are illustrated in Table 2.

Table 2. Remote-sensing data retrieved with their sources.

Year	Data Type	Source	Reference System	Number of Photos	Spatial Resolution	Datasets
2008	Orthomosaic	National Greek Cadastre	Hellenic Geodetic Reference System of 1987 (Greek Grid)	1	0.5 m	No further processing
2016	Orthomosaic	National Greek Cadastre	Hellenic Geodetic Reference System of 1987 (Greek Grid)	1	0.5 m	No further processing
2018	Worldview-2	Digital Globe	Universal Transverse Mercator Zone 34 (EPSG 32634)	1	0.50 m	Georeferenced to Hellenic Geodetic Reference System of 1987

The uncertainties, limitations and errors related to the shorelines extracted from maps and aerial photograph techniques have occupied the research community [71–73]. These refer to the five main routes of uncertainty during the shoreline vectorize procedure when using aerial photographs: seasonal error, tidal fluctuation error, digitizing error, pixel error and rectification error [72].

Seasonal and tidal fluctuation errors could considerate as negligible, since the images acquired during the summer seasons and the tide ranged from 0 to $\pm$ 10 cm, according to data derived from the online platform (https://www.worldtides.info/; accessed on: 30 September 2020) and the tide gauge system installed in the Gulf of Patras. As a relative example, we mention the high tide on the 18th of September 2018, the day of Worldview-2 image acquisition, which was estimated at almost 0.00 m. Considering the previous statement, any uncertainty is limited into the last three referred digitizing errors.

According to reference [74], the error associated with the pixel size of high-resolution imagery ranged from $\pm$ 0.3 to 1.0 m. As the datasets consist of high-resolution images with pixel sizes up to 0.5 m, we chose to proceed with the visual interpretation method. ERDAS IMAGINE 2014 and ArcMap v10.5 software were used for the processing of shoreline vectorizing, while DSAS application was used for the statistics and the assessment of the rate of change in every zone of the coastal area by computing the end point rates (EPR). The EPR calculates the rate of shoreline change dividing the distance between the oldest and most recent shorelines by the time elapsed [67].

After that, all digitized shorelines were produced in shapefiles and imported into a database in the ArcGIS platform in accordance with the Digital Shoreline Analysis System (DSAS v5.0) standards, such as the acquisition date, identity, shape, length and uncertainty [75]. The Digital Shoreline Analysis System is a tool that cooperates with the ArcMap software package and has been created by the United States Geological Survey. It is a popular tool, which calculates the changes in shoreline movements due to some various statistical rates [67]. Moreover, a smooth baseline was carefully created landward and used for the calculations. Several transects were created perpendicular to the baseline with fifty-meter intervals. The outlier rates were removed, and the remaining rates were statistically processed. With this tool, the vectorized shorelines for each zone were processed and computed as end point rates (EPR) for the period of 2008–2018.

The current study focused on the recent (last twelve years) evolution of the coastline, and for the specific period, we selected the most accurate available datasets. As described in Section 3.4, the three datasets used in the current study have a spatial resolution of 0.5m. The 2008 and 2016 are the official datasets of the Greek Cadastral. They are the most accurate datasets for the Greek territory. The 2018 worldview image also had a 0.5-m spatial resolution.

3.5. Average Tidal Range

According to Gornitz et al. [16], macro-tidal environments (big tidal range) are vulnerable to erosion, because they can create stronger currents and cause bigger sediment transportation in comparison with the micro-tidal environments. According to Thieler and Hammer-Klose [19] and Pendleton et al. [5], macro-tidal environments are considered as nonvulnerable due to the fact that during a storm surge in a micro-tidal coastal zone, the sea level is all the time close to a high tide and is more vulnerable to flooding.

The Gulf of Patras has been characterized as a micro-tidal environment, since the tidal change on the coasts is small. During this specific study, the small tide range ranked with low vulnerability, since the calculation of the CVI is against erosion and sea level rise and is not vulnerability against flooding and storm surges. The data and measurements of the tidal range in the Gulf of Patras were taken from a tide gauge system that has been installed in the port of Patras, with the average tidal range being equal to 0.24 m.

3.6. Sea Level Rise (SLR)

SLR is one of the consequences of climate change and global warming. According to the IPCC, the predicted sea level rise is expected to reach 1 m until 2100, and due to this, the coastal areas are high hazards. SLR is the annual mean increase or decrease water elevation measured at tide gauge stations, and the sea-level change along the Mediterranean coast is the sum of eustatic, glaciohydro-isostatic and tectonic factors [74].

In the Mediterranean Sea, the rate of sea level rise is 1.8 mm/year, as inferred from the analysis of tidal gauge data for the last century [76]. Galassi and Spada [77] extracted data from tide gauges placed along the Mediterranean shoreline (6 different cities) and observed SLR rates of a minimum of 0.64 to maximum 2.44 mm/year. In Greece, SLR due to eustatism is lower than 2 mm per year [78]. Based on these researches, the value of 1 mm/year was determined and taken as the most representative for the entire coastline of the study area. Same SLR value used in the research of Karymbalis et al. [24] for the assessment of the Coastal Sensitivity Index (CSI) in the Gulf of Corinth, which was located next to the Gulf of Patras.

3.7. CVI Calculation and Ranking

The initial step before the calculation of CVI, is to define the range values of each parameter to rank them with a specific vulnerability value; for example, "high or very high vulnerability. The ranges for the vulnerability ranking in Table 3 were derived from Karymbalis et al. [24] and Tragaki et al. [50]. However, the geotechnical characterization and its vulnerability ranking in Table 3 were presented for first time and gave a mostly accurate quantification of the resistance to erosion for this variable.

Table 3. Ranges of vulnerability ranking for each of the variables used in the Coastal Vulnerability Index (CVI) calculations.

Variables	Very Low (1)	Low (2)	Moderate (3)	High (4)	Very High (5)
Geotechnical Characterization	Rocky Coasts with High Cliffs	Soft Rocks/Hard Soils (Sandstone Coasts with Medium Cliffs)	Stiff-Hard Cohesive Soils (Low to Very Low Cliffs)	Cobble and Gravelly Coasts, D_{50} >2.50 mm (GP, GM, GP-GM)	Sandy Coasts, D_{50} < 2.50 mm (SM, SP, SW-SM ML)
Significant mean wave height (m)	<0.3	0.3–0.6	0.6–0.9	0.9–1.2	>1.2
Coastal slope (%)	>12	12–9	9–6	6–3	<3
Shoreline evolution (m/y)	>(+1.5)	(+1.5)–(+0.5)	(+0.5)–(−0.5)	(−0.5)–(−1.5)	<(−1.5)
Average tidal range (m)	<0.2	0.2–0.4	0.4–0.6	0.6–0.8	<0,8
Sea Level Rise (SLR) (mm/y)	<1.8	1.8–2.5	2.5–3.0	3.0–3.4	>3.4

As t mentioned before, for the calculations of the Coastal Vulnerability Index, two different methodologies and equations were used: (a) the general equation (CVI) of Gornitz et al. [16] and (b) a new (CVI$_{WF}$) by adding a weighted factor into the geotechnical characterization variable. Comparisons between the two different methodologies (CVI and CVI$_{WF}$) were performed. The two equations for the calculation of CVI and CVI$_{WF}$ are presented below:

$$CVI = \sqrt{\frac{a * b * c * d * e * f}{6}} \tag{1}$$

$$CVI_{WF} = \sqrt{\frac{a^3 * b * c * d * e * f}{6}} \tag{2}$$

where *a*: Geotechnical characterization, *b*: Significant mean height wave, *c*: Coastal slope, *d*: Shoreline evolution, *e*: Average tidal range and *f*: Sea Level Rise (SLR).

The final stage before the production of vulnerability maps is the ranking of the CVI values in the vulnerability classes. In the bibliography, researchers used different classification methods for giving vulnerability ranks in CVI values, such as equal intervals [7,16,30,79–81], natural breaks [22,24,25,50,82], percentiles [5,28,33,83–85] and standard deviation [51,86]. On this specific research, the equal interval classification method was chosen for ranking the CVI and CVI$_{WF}$ values.

4. Results

4.1. Geotechnical Characterization

The results for this variable show that more than half of the coastline of the Gulf of Patras is under a regime of very high vulnerability (52.29%), while high vulnerability covers 34.49% of the area (Figures 3 and 4). The results reveal that 52.29% of the coastline of the Gulf of Patras consists of materials that have very high vulnerability, i.e., materials of small grain sizes (sands with D_{50} < 2.50 mm) and poor geotechnical characteristics, while 34.49% is highly vulnerable and consists of materials of larger grain sizes (gravel with D_{50} > 2.50 mm). As moderately vulnerable characterizes 2.17% of the total coastline, while low and very low vulnerability characterizes 6.88% and 4.18% of the total coastline, respectively, consisting mainly of sandstone coasts with medium cliffs and rocky coasts with high cliffs.
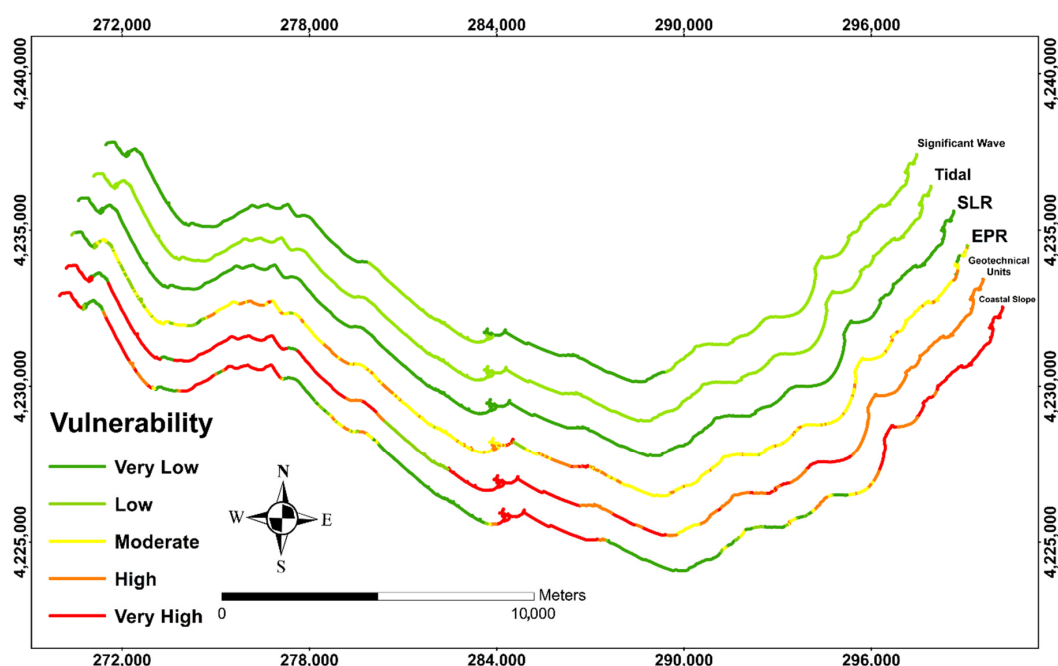

Figure 3. Spatial variations of each of the variables used in the Coastal Vulnerability Index (CVI) calculations along the coastline.
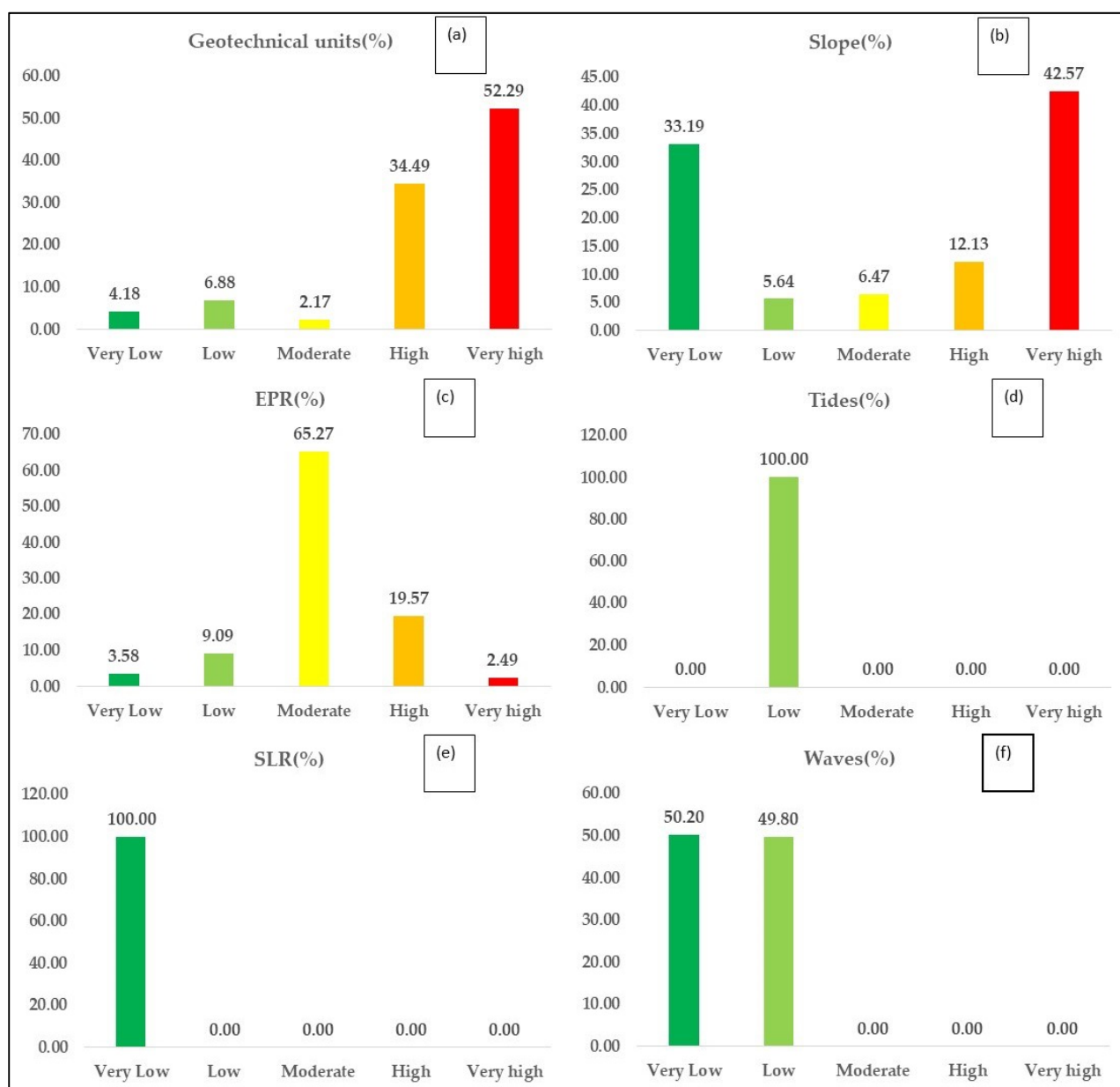
Figure 4. Vulnerability characterization in percentage (%) along the coastline of the pilot area for each of the variables used in the CVI calculations.

4.2. Significant Mean Wave Height

The survey area was divided into zones, and each of them received a specific value using the average value of the significant wave height occurring 40 m from the shoreline. Generally, the wave height in the Gulf of Patras is low, since it is a narrow gulf, where a high wind speed cannot be developed and generate waves with high heights. The results of the numerical simulation of wave propagation for wind speed with a return period of 10 years for each wind direction in the eight zones revealed that the maximum value of the wave heights was 0.53 m, whereas the minimum was 0.23 m. Similar values (0.3–0.4 m) of wave heights were extracted from the wave buoy, which was installed in the port of Patras. According to Table 3 (vulnerability ranks), values of wave heights lower than 0.3 m and values between 0.3 m and 0.6 m are ranked with a very low and low vulnerability, respectively. Based on this ranking, the 50.20% of the area is characterized with a very low

vulnerability, while 49.80% with low vulnerability (Figures 3 and 4). This is logical, since the gulf of Patras is not a wide sea to create higher waves.

4.3. Coastal Slope

Coastal slope values lower than 3% are characterized with very high vulnerability, and areas with values higher than 12% are characterized with very low vulnerability (Table 3). Values between 3% and 6% are characterized with high vulnerability, while values between 6–9% and 9–12% are characterized with moderate and low vulnerability, respectively (Table 3). The results from the calculation of the coastal slope variable show that most of the coastline (42.57%) is very high in vulnerability (gentle slopes), while 33.19% is described as very low in vulnerability (high slopes and rock masses). The remaining shoreline was calculated at 12.13%, 6.47% and 5.64% and was described as having high, medium and low vulnerabilities, respectively. The spatial variation of the coastal slope parameter along the study area is presented in the next paragraphs (Figures 3 and 4).

4.4. Shoreline Evolution

Shoreline evolution was estimated with the use of DSAS by computing a total of 773 transects along a land baseline in the eight zones of Figure 2 and producing the relevant EPR. Zone 1 has 184 transects and covers 10.80 km in length, the longest among all the zones. Zone 2 includes 60 transects and covers 3.02 km of coastal length. Zone 3 covers 7.31 km of coastal length considering 115 transects, whereas Zone 4 covers almost 4.43 km, and it has only 57 transects. Zone 5 extent up to 4.32 km with 82 transects, whereas Zone 6 has a length of 4.34 Km with 85 transects. Zone 7 consist of 78 transects with a length of 4.09 Km, while Zone 8 has 112 transects and covers 6.68 km in length. In zone 1, 64.67% of the transects reveal accretion and correspond to 6.96 Km in length.

In the western of zone 1, accretion with a rate over 1.50 m/y took place, whereas the majority of the transects showed a deposition (green color) with a rate that ranged from 0.50 to 1.00 m/y. Only in a small part of the eastern coast was erosion observed (orange color) with a rate that ranged from −1.00 to −1.50 m/y (Figure 9). Zones 2, 3 and 4 show erosion with rates of 81.67%, 80.00% and 70.18% of the relative transects, corresponding to 2.47 km, 5.85 km and 3.11 Km of littoral length. Erosion procedure dominated in zones 2 and 3 with a rate range from −1.00 to −1.50 m/y and from −0.50 to −1.00 m/y throughout almost the entire coast, while there were some places with severe erosion up to −1.50 m in both coasts (red color transects) (Figure 9). The similar rates of erosion were observed in zone 4 too, while there was a small area where accretion prevailed with a rate that ranges from 1.00 to 1.50 m/y (Figure 9).

Furthermore, in zones 5, 6, 7 and 8, it seems erosion rates are lower instead. Moreover, in these zones, there are parts where transects record values of EPR between −0.10 and +0.10 m/y (blue color) with significant rates such as 28.05%, 30.59%, 30.77% and 20.54%, which correspond to a distance of 1.21, 1.33, 1.26 and 1.37 km, respectively (Figure 10). These rates could be revealed stably, as they are very close to deviations of the statistical error. The highest shoreline change (erosion–accretion) according to the EPR rates was recorded as −2.57 m/year adjacent to zone 5 and +5.95 m/year in zone 1. Finally, although the overall trend of the shoreline according to the EPR rates is in agreement with those revealed from each zone, in zone 8, the shoreline trend recorded as accretion according to the mean EPR rates (+0.24 m/y) (Figure 10).

According to the ranges of vulnerability ranking for this variable (Table 3), the results revealed that the biggest part of the coastline (65.27%) has a moderate vulnerability, while a significant percentage (19.57%) has been assessed with a high vulnerability. The other vulnerability classes were estimated with a small percentage (very low 3.58%, low 9.09% and very high 2.49%) (Figures 3 and 4).

4.5. Average Tidal Range and SLR

The value of the tidal range for the entire coastline is equal to 0.24 m and is characterized with a low vulnerability (Figures 3 and 4). The value of the SLR is equal to 1 mm/year and is characterized with a very low vulnerability (Figures 3 and 4). Both the tidal range and SLR variables do not show any spatial variances, since they remain the same along the entire coastline (Figures 3 and 4).

4.6. Comparison between the CVI and CVI_{WF} Results

The percentage in each vulnerability class with the CVI application along the coastline of the research area was estimated as (a) very low vulnerable (20.13%), (b) low vulnerable (20.47%), (c) moderate vulnerable (24.56%), (d) high vulnerable (29.39%) and (e) very high vulnerable (5.45%). On the other hand, the percentage in each vulnerability class with the CVI_{WF} application is estimated as (a) very low vulnerable (14.59%), (b) low vulnerable (25.91%), (c) moderate vulnerable (20.04%), (d) high vulnerable (36.48%) and (e) very high vulnerable (2.98%) (Figure 5).

	CVI(%)	CVIWF(%)	Geotechnical (%)	Slope(%)	EPR(%)	SLR(%)	Tides(%)	Waves(%)
■ Very Low	20.13	14.59	4.18	33.19	3.58	100.00	0.00	50.20
■ Low	20.47	25.91	6.88	5.64	9.09	0.00	100.00	49.80
■ Moderate	24.56	20.04	2.17	6.47	65.27	0.00	0.00	0.00
■ High	29.39	36.48	34.49	12.13	19.57	0.00	0.00	0.00
■ Very high	5.45	2.98	52.29	42.57	2.49	0.00	0.00	0.00

Figure 5. Percentage in each vulnerability class in relation with the CVI and CVI_{WF} model applied in the research area.

In general, with the insertion of a weighted factor in the geotechncial parameter, an increase was observed in the low vulnerability class (CVI Class 2) and the high vulnerability class (CVI Class 4). At the same time, a decrease was observed in the very low vulnerability class (CVI Class 1), the moderate vulnerability class (CVI Class 3) and the very high vulnerability class (CVI Class 5) (Figure 6).
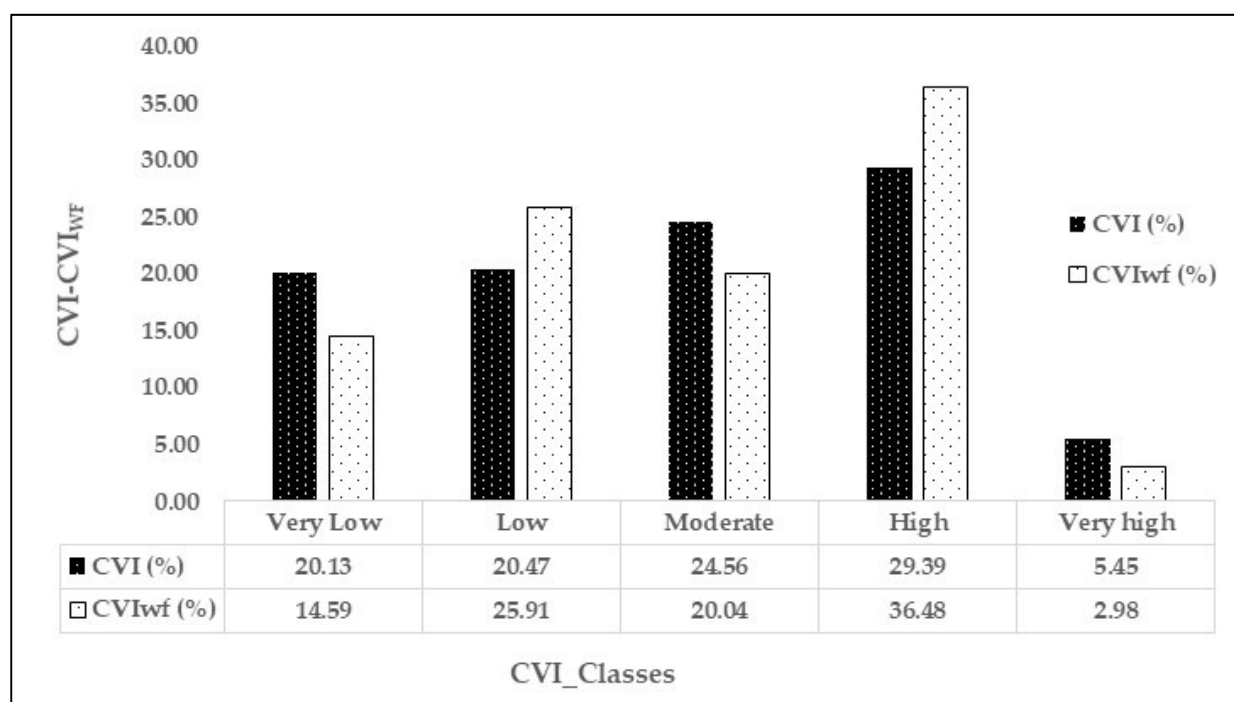
Figure 6. Comparison between the (CVI) and (CVI$_{WF}$) models applied in the research area.

The results of the spatial analysis from the CVI model application revealed that the areas that have very low vulnerability at erosion are Zones 2 and 5, low vulnerability, Zones 3 and 6, moderate vulnerability, Zones 1 and 4 and, finally, high vulnerability, Zones 7 and 8. On the other hand, the results of the spatial analysis from the CVI$_{WF}$ model application revealed that the areas that have very low vulnerability at erosions are Zone 3; low vulnerability, Zones 2, 5 and 6 and, finally, high vulnerability, Zones 1, 4, 7 and 8.

The results from the application of both models in the entire area of study (Zones 1–8) as a percentage (%) and length in Km for each one of the vulnerability classes are presented in Tables 4 and 5. A column chart of the vulnerability classes in Km for Zones 1–8 of the research area with the CVI and CVI$_{WF}$ applications is also presented in Figure 7.

Table 4. CVI and CVI$_{WF}$ results in Zones 1–4 of the research area.

CVI	Zone 1(km)	Zone 1(%)	Zone 2(Km)	Zone 2(%)	Zone 3(Km)	Zone 3(%)	Zone 4(km)	Zone 4(%)
Very Low	2.27	20.99	1.17	38.67	2.38	32.53	0.00	0.00
Low	2.07	19.14	0.83	27.42	2.52	34.50	0.00	0.00
Moderate	5.10	47.21	1.03	33.90	0.66	9.09	2.15	48.46
High	1.37	12.66	0.00	0.00	0.70	9.64	1.78	40.15
Very high	0.00	0.00	0.00	0.00	1.04	14.23	0.50	11.39
Total Km	10.80		3.02		7.31		4.43	
CVI$_{WF}$	**Zone 1(km)**	**Zone 1(%)**	**Zone 2(km)**	**Zone 2(%)**	**Zone 3(km)**	**Zone 3(%)**	**Zone 4(km)**	**Zone 4(%)**
Very Low	1.53	14.13	0.30	9.90	2.94	40.18	0.00	0.00
Low	2.45	22.71	1.75	57.75	1.70	23.22	0.00	0.00
Moderate	3.22	29.85	0.72	23.79	0.54	7.38	0.50	11.30
High	3.60	33.31	0.26	8.55	1.10	14.99	3.42	77.32
Very high	0.00	0.00	0.00	0.00	1.04	14.23	0.50	11.39
Total Km	10.80		3.02		7.31		4.43	

Table 5. CVI and CVI$_{WF}$ results in Zones 5–8 of the research area.

CVI	Zone 5(km)	Zone 5(%)	Zone 6(km)	Zone 6(%)	Zone 7(km)	Zone 7(%)	Zone 8(km)	Zone 8(%)
Very Low	3.11	71.92	0.09	1.97	0.00	0.00	0.00	0.00
Low	0.63	14.59	2.09	48.12	0.41	9.98	0.33	4.90
Moderate	0.41	9.59	1.57	36.24	0.14	3.48	0.15	2.27
High	0.17	3.90	0.59	13.67	3.22	78.63	5.34	79.97
Very high	0.00	0.00	0.00	0.00	0.32	7.91	0.86	12.86
Total Km	4.32		4.34		4.09		6.68	
CVI$_{WF}$	Zone 5(km)	Zone 5(%)	Zone 6(km)	Zone 6(%)	Zone 7(km)	Zone 7(%)	Zone 8(km)	Zone 8(%)
Very Low	1.68	38.86	0.14	3.14	0.00	0.00	0.00	0.00
Low	2.12	48.95	2.66	61.23	0.41	9.98	0.32	4.72
Moderate	0.51	11.86	1.26	29.01	0.84	20.61	1.12	16.74
High	0.01	0.34	0.29	6.62	2.73	66.75	5.25	78.54
Very high	0.00	0.00	0.00	0.00	0.11	2.65	0.00	0.00
Total Km	4.32		4.34		4.09			
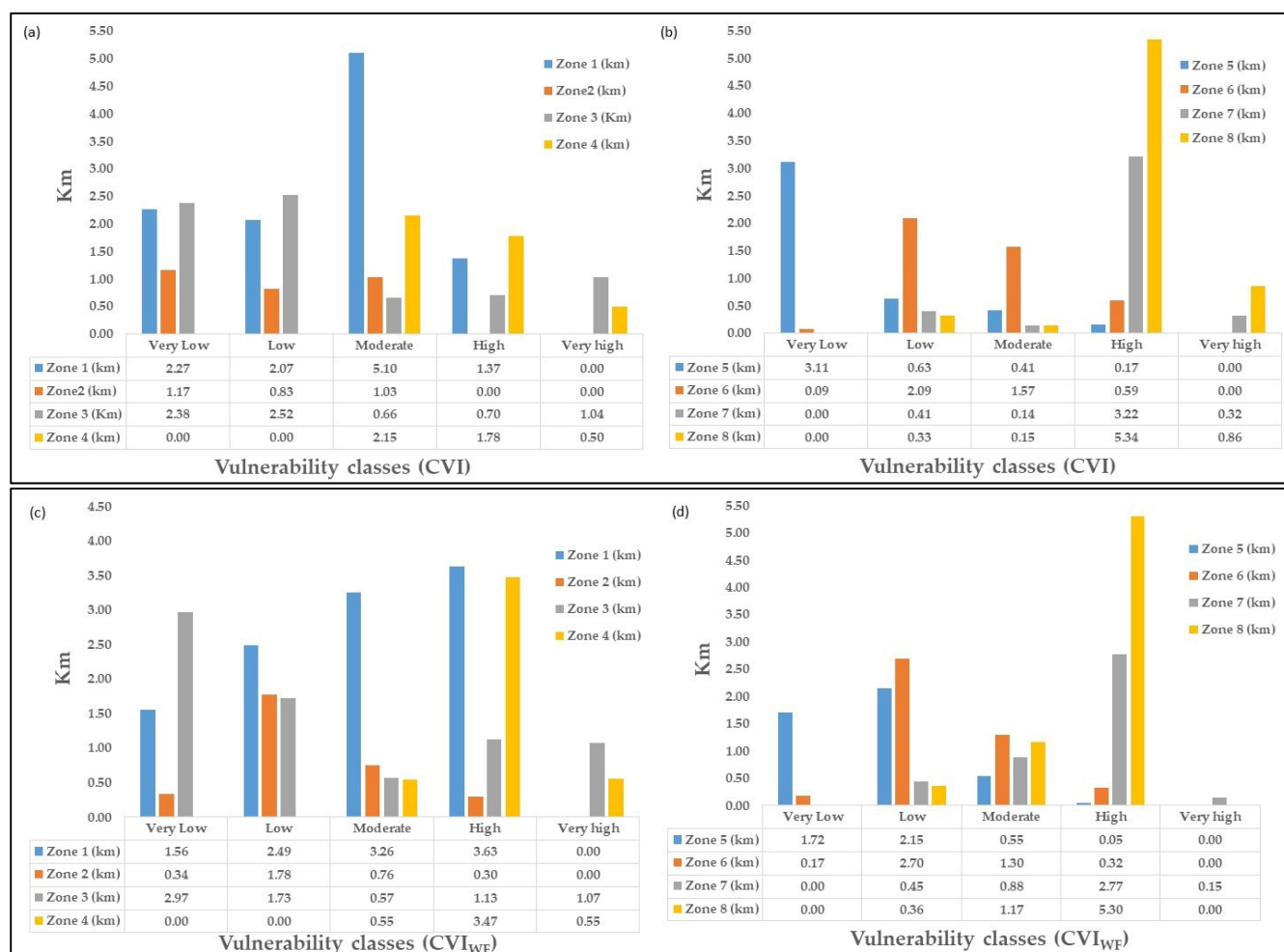
Figure 7. Column chart of the vulnerability classes in Km for Zones 1–8 of the research area with the CVI and CVI$_{wf}$ applications: (**a**) CVI classes in Zones 1-4, (**b**) CVI classes in Zones 5-8, (**c**) CVI$_{wf}$ classes in Zones 1–4, (**d**) CVI$_{wf}$ classes in Zones 5–8.

The range of CVI values alongside the shoreline of the gulf of Patras is between 0.82 and 8.17, with a mean value of 4.29 and standard deviation 1.71, whereas the range of the CVI$_{WF}$ values is between 0.82 and 40.82, with a mean value of 19.12 and standard deviation of 8.52 (Table 6).

Table 6. Statistics data of the CVI and CVI$_{WF}$ and ranges of the vulnerability classes.

Statistics	CVI	CVI$_{WF}$
Min.	0.82	0.82
Max.	8.17	40.82
Stdev.	1.71	8.52
Mean	4.29	19.12
Vulnerability Ranking	Range	Range
Very Low	0.82–2.29	0.82–8.82
Low	2.29–3.76	8.82–16.82
Moderate	3.76–5.23	16.82–24.82
High	5.23–6.7	24.82–32.82
Very high	6.7–8.17	32.82–40.82

4.7. Analysis on the Weighted Geotechnical Factor Applied on CVI$_{WF}$ Equation

As it has been mentioned before, a weighted geotechnical factor was added in the CVI$_{WF}$ equation in order to examine the importance of this parameter in the assessment of coastal vulnerability. The comparison between the CVI and CVI$_{WF}$ results (Figures 7 and 8) showed that the areas mostly affected by the weighted factor are (a) the Papa Lagoon–Karnari (Zone 1) and Alikes–Gialos (Zone 4), since they were assessed from a moderate vulnerability with the CVI to a high vulnerability with the CVI$_{WF}$ in their biggest parts, (b) the Karnari–Ioniki Akti (Zone 2) and Peiros–West Kaminia (Zone 5), since they were assessed from a very low vulnerability with the CVI to a low vulnerability with CVI$_{WF}$ in their biggest parts and (c) Ioniki Akti–West Alikes (Zone 3), since it was assessed from a low vulnerability with the CVI to a very low vulnerability with the CVI$_{WF}$ in its biggest part. The remaining Zones 6, 7 and 8 (from West kaminia to Glafkos) remained in their biggest parts with the same vulnerability (low in Zone 6 and high in Zones 7 and 8), regardless of the CVI or CVI$_{WF}$ applications. The spatial distribution of the CVI and CVI$_{WF}$ results alongside the coastline of the gulf of Patras is presented in detail in Figure 8.
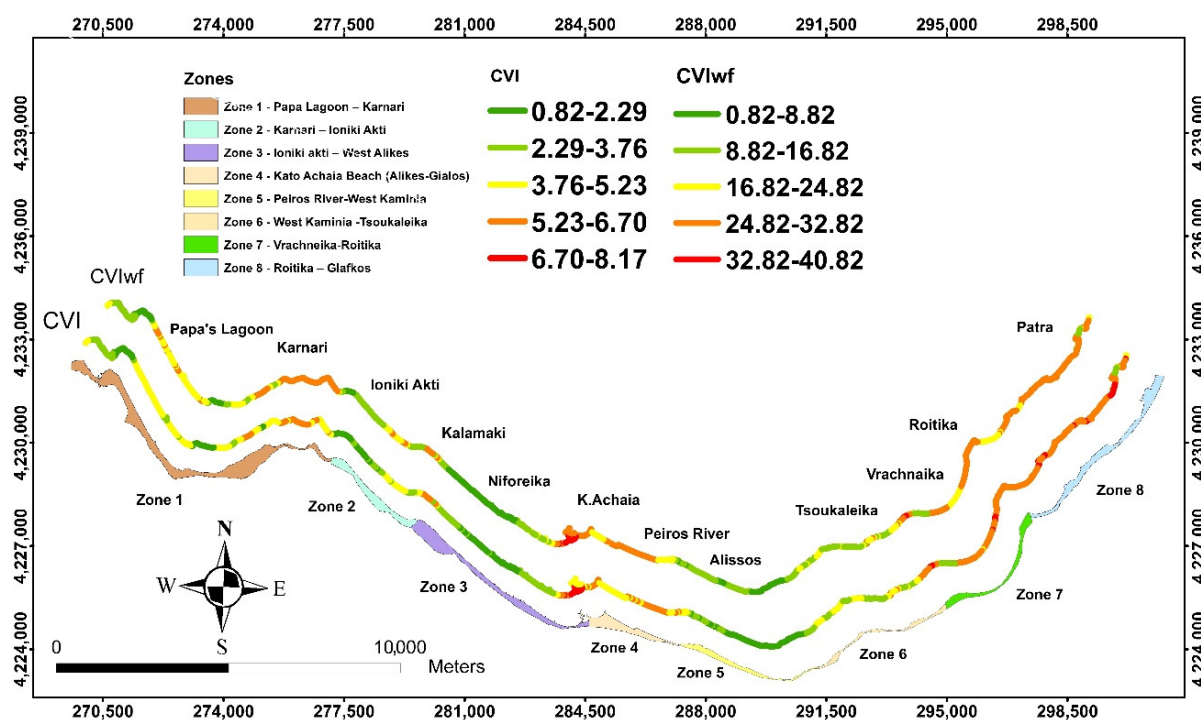
Figure 8. Spatial distribution of CVI and CVI$_{WF}$ alongside the shoreline of the Gulf of Patras.

By comparing the results from both equations, it seems that the CVI_{WF} equation is more realistic for this specific area, since it characterizes the eight zones more accurately in terms of their vulnerability at erosion. Especially, it characterizes more accurately the western part of the gulf (Zones 1, 2, 3 and 4), since this part is mostly affected by the SE winds; thus, the coastal erodibility and vulnerability should be higher, and this is evident with the CVI_{WF} results.

The geotechnical weighted factor decreased the vulnerability class on some segments of the coastline, which were mapped as cobble and gravel beaches ($D_{50} > 2.50$ mm) from high to moderate. On the contrary, an increase of the vulnerability class was observed on some segments of the coastline that were mapped as sandy beaches ($D_{50} < 2.50$ mm) from moderate to high. The addition of a weighted geotechnical factor in the CVI_{WF} equation changed the coastal vulnerability to a lower class in gravel and cobble beaches and a higher class in sandy beaches, which is more accurate for this particular area.

4.8. Analysis on the Computed EPR Values and the Respective CVI_{WF} Results

In Zone 1, the EPR shows that most of the coastline is under accretion, despite the fact of the existence of a geotechnical unit (fine sand) and a gentle coastal slope of very high vulnerability (CVI rank 5). However, in the eastern part of Zone 1 (Karnari Beach), erosion is observed with a rate ranging from -1.00 to -1.50 m/y, and this agrees mostly with the CVI_{WF} results (Figure 9). In Zone 2, the EPR reveals that most of the coastline is under erosion, with a rate ranging from -1.00 to -1.50 m/y. The CVI and CVI_{WF} results show this area as lowly vulnerable in its western part and moderate-to-highly vulnerable in its eastern part. Those differences between the CVI_{WF} and EPR is due to the steeper coastal slope and the rocky coast existing in the western part of Zone 2 (Figure 9). A lower erosion rate with an EPR -0.40 to -0.80 m/y exists in Zone 3, especially in the western and eastern parts, which decrease at -0.30 to 0.00 m/y in the central part. Both the CVI and CVI_{WF} results reveal high and very high vulnerabilities in the western and eastern parts of the zone, respectively, being in agreement with their respective EPR, which becomes a low vulnerability in the central part of the zone due to the existence of a higher coastal slope with soft rocks/hard soils (CVI rank 1) (Figure 9). In Zone 4, erosion dominates, apart from a very small accretion area in its central part. EPR is very high in the eastern part (-1.00 to -1.50 and > -1.50 m/y), where a dam was constructed upstream; thus, it blocks the sediment movement towards the coastline, and this agrees mostly with the CVI_{WF} results (Figure 9).
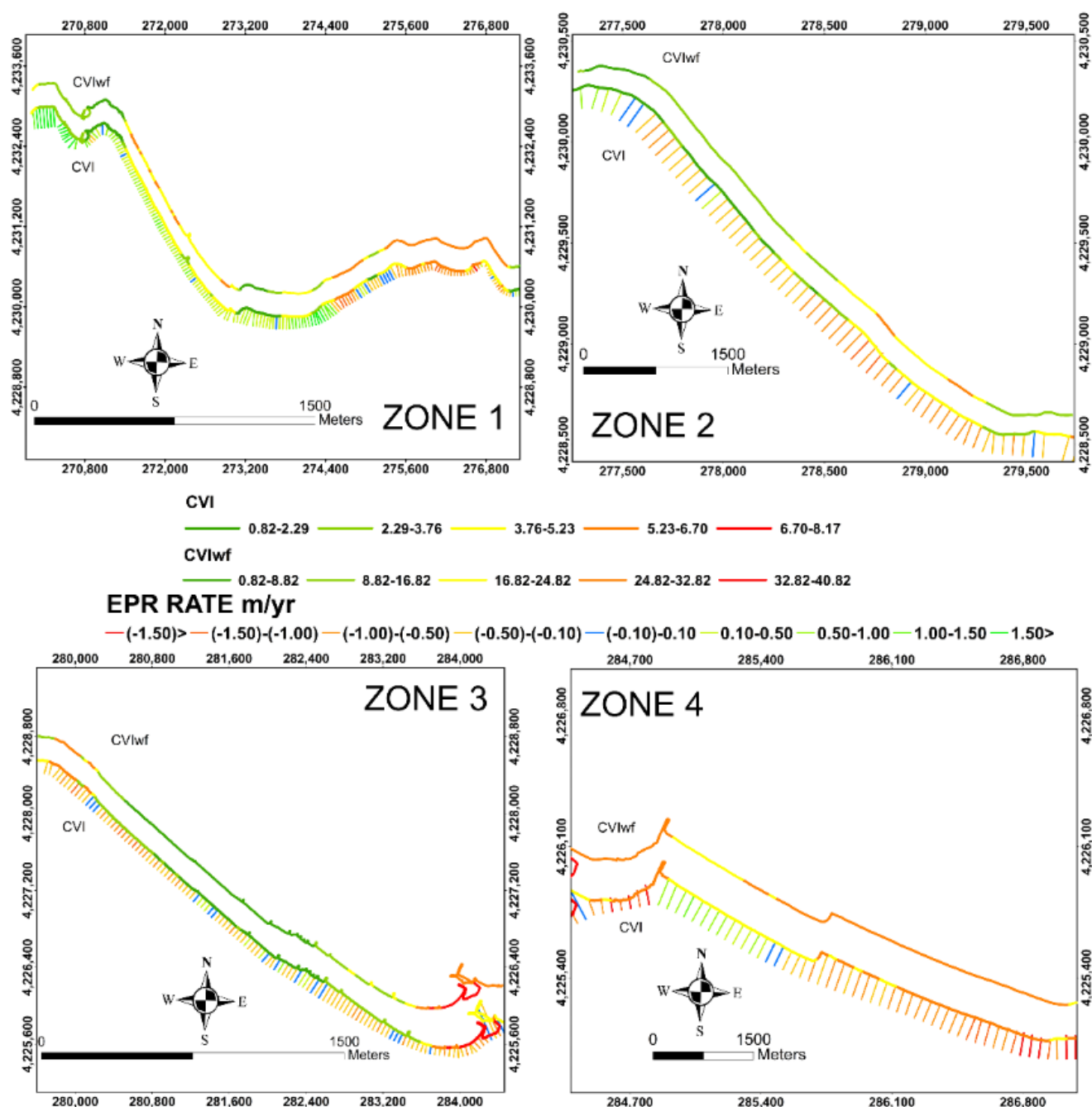
Figure 9. Comparison between the EPR and the vulnerability classes in Zones 1–4.

Zones 5, 6, 7 and 8 have smaller rates of erosion compared with Zones 1, 2, 3 and 4, with some parts characterized as stable shorelines (−0.10 to 0.10 m/y). Specifically, in Zone 5, its western part has a high rate of EPR (−1.00−−1.50 m/y), while most of the remaining area has smaller (−0.50−−0.00 m/y) and stabler rates (−0.10–0.10 m/y). Both the CVI and CVI_{WF} results revealed a low vulnerability because of the existence of a high coastal slope (CVI rank 1 and 2) with stiff–hard cohesive soils and medium cliffs (CVI rank 3). Zone 6 EPR has generally moderate rates and, in some parts, is stable (−0.10 to 0.10 m/y), while the results from both the CVI and CVI_{WF} reveal a low-to-moderate vulnerability, which, in general, agrees with the EPR values (Figure 10). The EPR in Zone 7 is similar with Zone 6, with most of its parts having moderate and high rates of erosion and some parts a stable rate of erosion. A comparison between the EPR and CVI_{WF} shows that most of the shoreline is under moderate/high erosion and vulnerability and generally match,

apart from a few segments, which were calculated with stable rates of the EPR (−0.10 to 0.10 m/y) (Figure 10). In Zone 8, the biggest part of the coastline has low EPR values, but in the eastern part of the zone is observed accretion. The CVI$_{WF}$ values agree only in some parts of this zone with the EPR, since the EPR rates show a low or stable erosional trend, and the vulnerability is calculated as moderate to high (Figure 10).
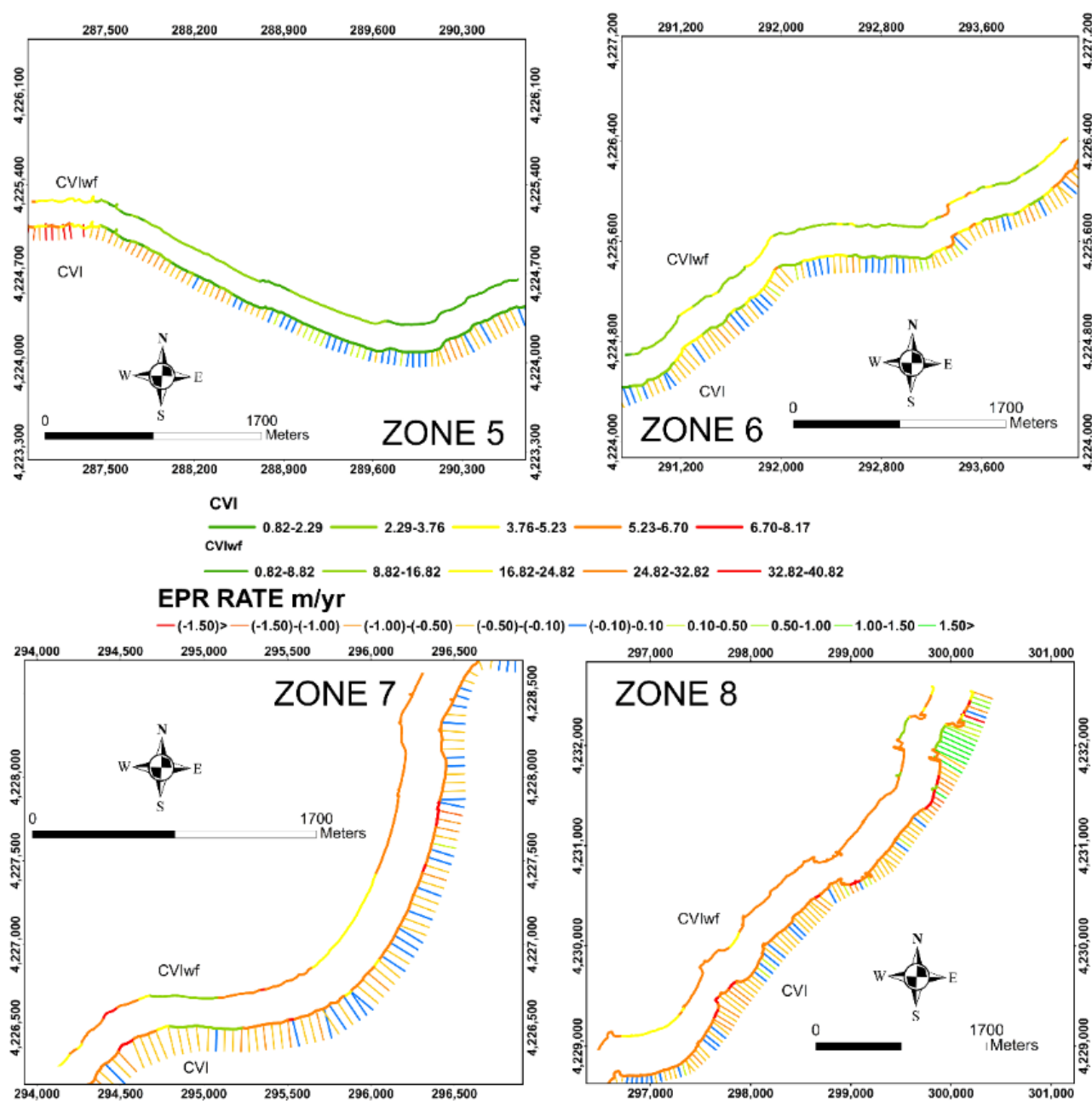

Figure 10. Comparison between the EPR and the vulnerability classes in Zones 5–8.

Weighted and unweighted vulnerability models have been tested for their appliance in the study area. For this purpose, the CVI and CVI$_{WF}$ models were compared with the calculated EPR values in each coastal segment. The main conclusion is that the historical evolution rate along the shoreline better suits the CVI$_{WF}$ model. As a result, the second estimation (with CVI$_{WF}$) seems to be more realistic, since it coordinates better with the EPR and historical evolution rate of the shoreline.

Specifically, in Zone 1, the eastern part (Karnari), the EPR values are in the biggest agreement with the CVI_{WF} rather than the CVI results (Figure 9). In Zone 2, the EPR and CVI_{WF} are closer to their results, especially in the central part of the zone (Figure 9). Zones 3 and 4 have a similar behavior between the EPR, CVI and CVI_{WF} results, apart from a few segments where the EPR and CVI_{WF} have better agreement (Figure 9). In Zones 5 and 6, the results of the CVI and CVI_{WF} are similar with the EPR values, except for a few segments where the CVI has a better agreement with the EPR (Figure 10). In Zone 7, the EPR values are in the biggest agreement with the CVI_{WF} rather than CVI (Figure 10), while in Zone 8, the EPR values in some parts are closer with the CVI and, in other parts, are closer to the CVI_{WF} (Figure 10).

5. Discussion

Among a variety of other indicators and methodologies, the Coastal Vulnerability Index (CVI) was chosen as a method for estimation and calculation of the vulnerability against sea erosion in the pilot area of the Gulf of Patras in Western Greece, due to its multiple advantages compared with other techniques. Another reason is that it is a very productive, low-cost and efficient tool for coastal hazard mapping and management. Thus, it gives a quick identification of erosion hotspots in order to enhance coastal engineers and local authorities to facilitate suitable management and coastal protection plans, the regulation of coastal zones and adaption strategies against erosion. However, the CVI approach reveals many uncertainties and doubts and, consequently, can bring wrong results in the vulnerability analysis. These uncertainties must be defined, improved and modified before any vulnerability calculations in order to increase the accuracy and reliability of the results. In the present study, to overcome the aforementioned problems, the following steps were conducted: (1) the use of geotechnical data instead of geological–geomorphological data, (2) the use of high-resolution remote-sensing data and (3) the insertion of a geotechnical weighted factor in the CVI formula. Finally, for the better understanding and evaluation of erosion analysis and vulnerability detection, as well as the efficiency of the CVI_{WF} on these calculations, comparisons between the CVI and CVI_{WF} results and with the EPR rates were performed.

A first attempt towards the improvement and quantification of resistance to erosion with CVI calculations was performed in this research with the use of the geotechnical parameter instead of the geological–geomorphological parameter. Instead of the classical qualitative methodologies using just the rock type or the geomorphology feature, the use of geotechnical data for the characterization of the coastal formations has proven to be a more reliable and accurate method to assess the resistance of a coastal formation to erosion. Only a few researchers have used geotechnical methods for the estimation of the CVI, such as Ruzic et al. [29], with the application of the Geological Strength Index (GSI) in order to calculate the quality of limestone rock masses in Croatia. Due to that, it is necessary to conduct more research on this variable, since it is maybe the most important variable that affects coastal erosion. The proposed modified CVI_{WF} model is a first attempt to introduce geotechnical aspects in the erosion vulnerability detection, since only a small number of papers have been published on this topic. From this research, it can be stated that the geotechnical characterization for CVI calculations is mainly based on the physical and mechanical characteristics of soils derived from borehole drilling, in-situ and laboratory tests, as well as sediment sampling. This type of characterization uses the soil's granulometry, geotechnical designation and the resistance to SPT measurements, which, in total, provide a more accurate measure of the soil's penetration resistance.

Another important variable that proved to be very important in the determination of the coastal vulnerability is the shoreline evolution, otherwise known as the historical shoreline change rate, with the application of extensive remote-sensing techniques. Generally, there are two main categories of studies regarding remote-sensing monitoring: those that they use free-of-charge low-resolution data and those that use high-resolution data. Over time, many studies have tried to process shoreline evolution with low-resolution satellite

images, but their results that emerged always had a lack of accuracy. Different methods have been used to overpass this drawback regarding the accuracy of the measurements and the results they provide. Pardo Pasqual et al. [53] developed a very complicated methodology in order to ameliorate the Landsat data accuracy using high-resolution air photo mosaic by co-registering the low-resolution coastline derived from Landsat data to the respective high-resolution shoreline. In another similar study, Almonacid et al. [60] computed the average annual coastline movement of many Landsat images and yield a mean error of −4.7 m, showing that the shorelines derived from Landsat images are placed seaward in comparison to the respective high-precision shorelines. In a recent study in Northwestern Peloponnese, Apostolopoulos and Nikolakopoulos [57] followed a statistical analysis using the Digital Shoreline Analysis System (DSAS) software and concluded that low-resolution data are not suitable either for shoreline forecasting or shoreline mapping, as their accuracy were very low, as they presented a divergence that ranges between 6 and 11 m. In a similar study, Apostolopoulos et al. [58] concluded that the accuracy of the vector data derived from Sentinel-2 10-m spatial resolution images ranged between 1 and 5 m using the NDVI and NDWI indices, respectively. On the other hand, the synergy of high-resolution satellite imagery and high-scale aerial photos has become a very accurate combination in order to study the coastal zone changes. In the current study, the shore-line rate of change was computed based on high-resolution aerial and satellite images, improving the rate's accuracy. These datasets were processed in a GIS platform, and the statistical analysis was performed through DSAS application by computing the EPR. The use of high-resolution data provided an improved accuracy in the CVI analysis and gave better results in finding the respective erosion or accretion trends along the shoreline.

The original formula for the CVI computation did not include weighted factors, and this was mentioned as a big disadvantage of the method, since the parameters do not all have the same importance. However, not a big number of researchers put in their vulnerability analysis weighted variables. The calculation of weighted factors can be done either arbitrarily by the specialist who develops the model or with various semi-quantitative methods, such as the Analytical Hierarchical process (AHP). In the current study, the weighted factor was added arbitrarily to the geotechnical variable only, since that specific variable seemed to be one of the most important in the CVI calculations. Initially, the CVI_{WF} was calculated with a squared power (a^2) weighted factor of the geotechnical variable, but the results were similar with those of the unweighted factor index. Hence, the cubed weighted factor (a^3) was chosen in the CVI_{WF} formula. By comparing the results from both equations CVI and CVI_{WF} (a^3), it was concluded that the CVI_{WF} is more realistic, since it characterized the eight zones of the investigation area more accurately in terms of their vulnerability at erosion. This was also analyzed in Section 4.8 (analysis on the computed EPR values and the respective CVI_{WF} results). The same procedure was followed by Rao et al. [7], who added weighted parameters in the CVI formula in the variables of geomorphology, coastal slope and coastal change, while Ruzic et al. [29] used weighted factor only in the geological parameter. New studies have calculated the weighted factors by using more advanced techniques, such as the Analytical Hierarchical process (AHP) [30,31,87–90]. In any case, the introduction of weighted factors in the CVI models is now necessary in order to calculate more accurately the coastal vulnerability; thus, the results can be derived by coastal engineers and managers for making the right decisions to mitigate the erosion phenomenon.

In order to compare which model CVI or CVI_{WF} is more accurate and closer to reality, a direct comparison between the two vulnerability indexes (unweighted and weighted) and the EPR values was performed (Figures 9 and 10). Both methods predict the degree of vulnerability to erosion very well, but the second model CVI_{WF} with the geotechnical weighted factor seemed to be more realistic, since it agreed with the rate of shoreline change in most of the coastal segments. This means that the geotechnical parameter affected the coastal vulnerability to a very high degree and especially in areas without high waves and SLR (such as the Gulf of Patras) and, therefore, may be one of the most important

variables that controls vulnerability to erosion. Hence, the geotechnical properties and characterization of the coastal zones must be defined for the better and higher accuracy of the predicted vulnerability indexes and must be included in the CVI computations instead of the parameter of geology.

De Serio et al. [30] calculated the CVI with and without weighted factors and concluded that the unweighted CVI underestimated the vulnerability, while the weighted seemed to be more realistic, which agrees with the conclusions of this research. Bagdanaviciute et al. [88] also ran the CVI with weighted factors that led to an increase in the very high vulnerability class provided with this way higher accuracy and more consistent results compared with the unweighted CVI.

Similar studies based on indexes for the estimation of vulnerability to coastal erosion, to SLR, to flooding, etc. have been performed in many countries with reliable results. Toressan et al. [49] assessed the relative vulnerability of the Mediterranean shoreline of Egypt by using a Climate-improved Coastal Vulnerability Index (CCVI) evaluating the potential effects of climate change in the assessment of coastal hazards. Perez and Selvaraj [84] applied the same model in the district of Buenaventura in West Colombia using eight variables, while Hereher et al. [91] used the Coastal Vulnerability Index for the estimation of susceptibility in Oman with the implementation of five physical parameters. This index-based methodology was applied also in Spain, where a comparison study between different CVI approaches was performed in Barcelona [27], and in the Valdelagrana area, Rizzo et al. [92] determined the coastal susceptibility to erosion and flooding processes by means of an index-based method. Audere and Robin [93] presented an assessment of the vulnerability to erosion of sandy coasts of Vendee (Western France) using long-term measurements of the historical evolution of the shoreline between 1950 and 2016 and short-term measurements caused by extreme events. In China, Zhang et al. [94] developed a composite Vulnerability Index in a coastline of 5627 Km using biophysical, sensitivity and adaptivity variables.

The extensive descriptions in the literature of these models prove that vulnerability models with the combined action of an index and Geographical Information Systems (GIS) are among the most widely used methodologies for the assessment of coastal vulnerability. Their use in many areas and their reference by many researchers shows that it is a reliable method, but it also needs many improvements that need to be clarified, some of which were attempted to be clarified in this work.

6. Conclusions

The aim of the present study was the estimation of Coastal Vulnerability Index using only physical factors in the pilot area of the Gulf of Patras in Western Greece in order to give prominence to the importance of geotechnical evaluation and shoreline evolution in CVI calculations. For this reason, the CVI index modified the replacement of the geological parameter with that of geotechnical characterizations. In addition, the modifications included the introduction of a weighted factor in the original CVI formula in the new geotechnical parameter and the use of remote-sensing data of high resolution, for better and more reliable results in the calculation of the historical shoreline changes with the EPR analysis. The data inserted in the Geographical Information System (GIS) and the CVI calculated for the entire coastline of the pilot area was divided into 50-m coastal segments.

According to the results, with the insertion of a weighted factor in the geotechnical parameter, an increase in CVI Class rates was observed in the low vulnerability class (from 20.47% to 25.91% in Class 2) and the high vulnerability class (from 29.39% to 36.48% in Class 4). At the same time, a decrease was observed in the very low vulnerability class (from 20.13% to 14.59% in Class 1), the moderate vulnerability class (from 24.56% to 20.04% in Class 3) and the very high vulnerability class (from 5.45% to 2.98% in Class 5). By comparing the results from both equations, it seems that the CVI_{WF} equation is more realistic for this specific area, since it characterizes the eight zones of the pilot area more accurately in terms of their vulnerability at erosion. Especially, it characterizes more

accurately the western part of the gulf (Zones 1, 2, 3 and 4), since this part is mostly affected by the SE winds; thus, the coastal erodibility and vulnerability were found to be higher in those zones with the performed CVI$_{WF}$ calculations.

Furthermore, EPR calculated rates revealed that most of the coastline in the study area is under erosion, with mean rates that range from -0.27 to -0.90 m/y, but in some parts, higher erosion rates were computed. Zone 1 is the only area that accretion processes dominate against erosion, whereas the erosion process dominates in all the other zones (Zones 2–8). In general, the results of the CVI$_{WF}$ model are identical to the erosion hotspot calculated with the EPR values apart from a few parts where the variable of the coastal slope is high and, as a result, decreases the vulnerability. A comparison between the EPR values and CVI-CVI$_{WF}$ models revealed that the second model of the unweighted method is closer and more realistic for a vulnerability assessment. This fact shows that the variable of geotechnical characterization is important and must be included in vulnerability calculations. However, geotechnical data are not easy to obtain, since they demand experienced personnel and in-situ and lab equipment. In addition, it is difficult to evaluate geotechnical data that have been performed along a very long shoreline for CVI calculations because (a) it is a very complex issue and (b) there are not many papers in the bibliography with the integration of the geotechnical parameter in CVI models. Therefore, on this research, a first attempt towards this direction was made in order to demonstrate the importance of the geotechnical parameter on coastal erosion processes and vulnerability. The next stage of this methodology could be the addition of geotechnical data with higher accuracy in order to develop a holistic approach of the geotechnical aspect in CVI models.

Although the pilot area's coastline is largely composed of materials prone to erosion and with gentle slopes, it was not assessed with a high percentage of high and very high vulnerability on the entire coastline, because the Gulf of Patras is a micro-tidal environment with low wave heights and a small sea level rise rate. However, in a possible change of those hydrodynamic parameters, due to the climate change, the regime of vulnerability will increase dramatically. Due to that, it is significant and necessary to systematically monitor this phenomenon and record in detail the observed values from all the parameters.

References

1. IPCC. Global Warming of 1.5°C. Available online: https://www.ipcc.ch/sr15/ (accessed on 30 September 2020).
2. EUROSION. *Living with Coastal Erosion in Europe: Sediment and Space for Sustainability*; European Environment Agency: Copenhagen, Denmark, 2004.
3. Ramieri, E.; Hartley, A.; Barbanti, A.; Duarte Santos, F.; Gomes, A.; Hilden, M.; Laihonen, P.; Marinova, N.; Santini, M. *Methods for Assessing Coastal Vulnerability to Climate Change*; ETC CCA Technical Paper; European Environment Agency: Copenhagen, Denmark, 2011.
4. ESTAT. *Nearly Half of the Population of EU Countries With a sea Border is Located in Coastal Regions*; EUROSTAT: Luxembourg, 2009.
5. Pendleton, E.A.; Thieler, E.R.; Williams, S.J.; Beavers, R.S. *Coastal Vulnerability Assessment of Padre Island National Seashore (PAIS) to Sea-Level Rise*; US Geological Survey Open-File Report; U.S. Geological Survey: Woods Hole, MA, USA, 2004.
6. McEvoy, S.; Haasnoot, M.; Biesbroek, R. How are European countries planning for sea level rise? *Ocean Coast. Manag.* **2021**, *203*, 105512. [CrossRef]
7. Rao, K.N.; Subraelu, P.; Rao, T.V.; Malini, B.H.; Ratheesh, R.; Bhattacharya, S.; Rajawat, A. Sea-level rise and coastal vulnerability: An assessment of Andhra Pradesh coast, India through remote sensing and GIS. *J. Coast. Conserv.* **2008**, *12*, 195–207. [CrossRef]
8. Falck, A.; Skramstad, E.; Berg, M. Use of QRA for decision support in the design of an offshore oil production installation. *J. Hazard. Mater.* **2000**, *71*, 179–192. [CrossRef]
9. Bolado, R.; Gracceva, F.; Zeniewski, P.; Zastera, P.; Vanhoorn, L.; Mengolini, A. *Best Practices and Methodological Guidelines for Conducting Gas Risk Assessments*; European Commission: Luxembourg, 2012. [CrossRef]
10. Di Risio, M.; Bruschi, A.; Lisi, I.; Pesarino, V.; Pasquali, D. Comparative Analysis of Coastal Flooding Vulnerability and Hazard Assessment at National Scale. *J. Mar. Sci. Eng.* **2017**, *5*, 51. [CrossRef]
11. Di Risio, M.; Lisi, I.; Beltrami, G.; De Girolamo, P. Physical modeling of the cross-shore short-term evolution of protected and unprotected beach nourishments. *Ocean Eng.* **2010**, *37*, 777–789. [CrossRef]
12. Skogdalen, J.E.; Vinnem, J.E. Quantitative risk analysis of oil and gas drilling, using Deepwater Horizon as case study. *Reliab. Eng. Syst. Saf.* **2012**, *100*, 58–66. [CrossRef]
13. UNEP/MAP/RAC-PAP. In *Mediterranean Protocol, Protocol on Integrated Coastal Zone Management in the Mediterranean*; UNEP/MAP/RAC-PAP: Athens, Greece, 2008. [CrossRef]
14. European Commission. *Proposal for a Directive of the European Parliament and the Council Establishing a Framework for Maritime Spatial Planning and Integrated Coastal Management*; European Commission: Luxembourg, 2013.
15. Bruno, M.F.; Saponieri, A.; Molfetta, M.G.; Damiani, L. The DPSIR Approach for Coastal Risk Assessment under Climate Change at Regional Scale: The Case of Apulian Coast (Italy). *J. Mar. Sci. Eng.* **2020**, *8*, 531. [CrossRef]
16. Gornitz, V. Global coastal hazards from future sea level rise. *Glob. Planet. Chang.* **1991**, *3*, 379–398. [CrossRef]
17. Gornitz, V.M.; Daniels, R.C.; White, T.W.; Birdwell, K.R. The Development of a Coastal Risk Assessment Database: Vulnerability to Sea-Level Rise in the U.S. Southeast. *J. Coast. Res.* **1994**, *12*, 327–338.
18. Thieler, E.R.; Hammar-Klose, E.S. *National Assessment of Coastal Vulnerability to Sea-Level Rise*; Technical Report; U.S. Geological Survey: Woods Hole, MA, USA, 1999.
19. Thieler, E.R.; Hammar-Klose, E.S. *National Assessment of Coastal Vulnerability to Sea-Level Rise; Preliminary Results for the US Pacific Coast*; Technical Report; U.S. Geological Survey: Woods Hole, MA, USA, 2000.
20. Doukakis, E. Coastal vulnerability and risk parameters. *Eur. Water* **2005**, *11*, 3–7.
21. Diez, P.G.; Perillo, G.M.; Piccolo, M. Vulnerability to sea-level rise on the coast of the Buenos Aires Province. *J. Coast. Res.* **2007**, *23*, 119–126. [CrossRef]
22. Gaki-Papanastassiou, K.; Karymbalis, E.; Serafim, P.; Zouva, C. Coastal vulnerability assessment to sea-level rise based on geomorphological and oceanographical parameters: The case of Argolikos GulfGulf, Peloponnese, Greece. *Hell. J. Geosci.* **2010**, *45*, 109–122.
23. Ozyurt, G.; Ergin, A. Improving Coastal Vulnerability Assessments to Sea-Level Rise: A New Indicator-Based Methodology for Decision Makers. *J. Coast. Res.* **2010**, *26*, 265–273. [CrossRef]
24. Karymbalis, E.; Chalkias, C.; Chalkias, G.; Grigoropoulou, E.; Manthos, G.; Ferentinou, M. Assessment of the Sensitivity of the Southern Coast of the GulfGulf of Corinth (Peloponnese, Greece) to Sea-level Rise. *Open Geosci.* **2012**, *4*, 561–577. [CrossRef]
25. Karymbalis, E.; Chalkias, C.; Ferentinou, M.; Chalkias, G.; Magklara, M. Assessment of the Sensitivity of Salamina and Elafonissos islands to Sea-level Rise. *J. Coast. Res.* **2014**, *70*, 378–384. [CrossRef]
26. Benassai, G.; Di Paola, G.; Aucelli, P.P.C. Coastal risk assessment of a micro-tidal littoral plain in response to sea level rise. *Ocean Coast. Manag.* **2015**, *104*, 22–35. [CrossRef]
27. Koroglu, A.; Ranasinghe, R.; Jiménez, J.A.; Dastgheib, A. Comparison of coastal vulnerability index applications for Barcelona Province. *Ocean Coast. Manag.* **2019**, *178*, 104799. [CrossRef]
28. Pramanik, M.K.; Biswas, S.S.; Mondal, B.; Pal, R. Coastal vulnerability assessment of the predicted sea level rise in the coastal zone of Krishna–Godavari delta region, Andhra Pradesh, east coast of India. *Environ. Dev. Sustain.* **2016**, *18*, 1635–1655. [CrossRef]
29. Ružic, I.; Jovancevic, D.; Benac, C.; Krvavica, N. Assessment of the Coastal Vulnerability Index in an Area of Complex Geological Conditions on the Krk Island, Northeast Adriatic Sea. *Geosciences* **2019**, *9*, 219. [CrossRef]
30. De Serio, F.; Armenio, E.; Mossa, M.; Petrillo, A.F. How to define priorities in coastal vulnerability assessment. *Geosciences* **2018**, *8*, 415. [CrossRef]

31. Zhu, Z.T.; Cai, F.; Chen, S.L.; Gu, D.Q.; Feng, A.P.; Cao, C.; Qi, H.H.; Lei, G. Coastal vulnerability to erosion using a multi-criteria index: A case study of the Xiamen coast. *Sustainability* **2019**, *11*, 93. [CrossRef]

32. Greco, M.; Martino, G. Vulnerability assessment for preliminary flood risk mapping and management in coastal areas. *Nat. Hazards* **2016**, *82*, 7–26. [CrossRef]

33. López Royo, M.; Ranasinghe, R.; Jiménez, J.A. A rapid, low-cost approach to coastal vulnerability assessment at a national level. *J. Coast. Res.* **2016**, *32*, 932–945. [CrossRef]

34. IPCC. International Panel on Climate Change. AR4 Climate change: The physical science basis. In *Contribution of Working Group I to the Fourth Assessment Report of the Intergovernmental Panel on Climate Change*; Solomon, S., Qin, D., Manning, M., Chen, Z., Marquis, M., Averyt, K.B., Tignor, M., Miller, H.L., Eds.; Cambridge University Press: Cambridge, UK, 2007.

35. Rangel-Buitrago, N.; Neal, W.; Jonge, V. Risk assessment as tool for coastal erosion management. *Ocean Coast. Manag.* **2020**, *186*, 105099. [CrossRef]

36. Kantamaneni, K.; Rani, S.; Rice, L.; Sur, K.; Thayaparan, M.; Kulatunga, U.; Rege, R.; Yenneti, K.; Campos, L. A Systematic Review of Coastal Vulnerability Assessment Studies along Andhra Pradesh, India: A Critical Evaluation of Data Gathering, Risk Levels and Mitigation Strategies. *Water* **2019**, *11*, 393. [CrossRef]

37. Bukvic, A.; Rohat, G.; Apotsos, A.; Sherbinin, A. Systematic Review of Coastal Vulnerability Mapping. *Sustainability* **2020**, *12*, 2822. [CrossRef]

38. Anfuso, G.; Postacchini, M.; Luccio, D.; Benassai, G. Coastal Sensitivity/Vulnerability Characterization and Adaptation Strategies: A Review. *J. Mar. Sci. Eng.* **2021**, *9*, 72. [CrossRef]

39. Cutter, S.L.; Boruff, B.J.; Shirley, W.L. Social vulnerability to environmental hazards. *Soc. Sci. Q.* **2003**, *84*, 242–261. [CrossRef]

40. Preston, B.L.; Smith, T.F.; Brooke, C.; Gorddard, R.; Measham, T.G.; Withycombe, G.; McInnes, K.; Abbs, D.; Beveridge, B.; Morrison, C. *Mapping Climate Change Vulnerability in the Sydney Coastal Group*; CSIRO Marine and Atmospheric Research: Canberra, Australia, 2008; 124p.

41. Satta, A.; Puddu, M.; Venturini, S.; Giupponi, C. Assessment of coastal risks to climate change related impacts at the regional scale: The case of the Mediterranean region. *Int. J. Disaster Risk Reduct.* **2017**, *24*, 284–296. [CrossRef]

42. Satta, A.; Snoussi, M.; Puddu, M.; Flayou, L.; Hout, R. An index-based method to assess risks of climate-related hazards in coastal zones: The case of Tetouan. Estuar. *Coast. Shelf Sci.* **2016**, *175*, 93–105. [CrossRef]

43. Kantamaneni, K.; Phillips, M.; Thomas, T.; Jenkins, R. Assessing coastal vulnerability: Development of a combined physical and economic index. *Ocean Coast. Manag.* **2018**, *158*, 164–175. [CrossRef]

44. McLaughlin, S.; Cooper, J.A.G. A multi-scale coastal vulnerability index: A tool for coastal managers? *Environ. Hazards* **2010**, *9*, 233–248. [CrossRef]

45. Zanetti, V.; de Sousa Junior, W.; De Freitas, D. A climate change vulnerability index and case study in a Brazilian coastal city. *Sustainability* **2016**, *8*, 811. [CrossRef]

46. Narra, P.; Coelho, C.; Sancho, F. Multicriteria GIS-based estimation of coastal erosion risk: Implementation to Aveiro sandy coast, Portugal. *Ocean Coast. Manag.* **2017**, *178*, 104845. [CrossRef]

47. Serafim, M.B.; Siegle, E.; Corsi, A.C.; Bonetti, J. Coastal vulnerability to wave impacts using a multi-criteria index: Santa Catarina (Brazil). *J. Environ. Manag.* **2019**, *230*, 21–32. [CrossRef] [PubMed]

48. Szlafsztein, C.; Sterr, H. A GIS-based vulnerability assessment of coastal natural hazards, state of Pará, Brazil. *J. Coast. Conserv.* **2007**, *11*, 53–66. [CrossRef]

49. Torresan, S.; Furlan, E.; Critto, A.; Michetti, M.; Marcomini, A. Egypt's coastal vulnerability to sea level rise and storm surge. Present and Future Conditions. *Integr. Environ. Assess. Manag.* **2020**, *16*, 761–772. [CrossRef] [PubMed]

50. Tragaki, A.; Gallousi, C.; Karymbalis, E. Coastal hazard vulnerability assessment based on geomorphic, oceanographic and demographic parameters: The case of the Peloponnese (Southern Greece). *Land* **2018**, *7*, 56. [CrossRef]

51. Alexandrakis, G.; Poulos, S. An holistic approach to beach erosion vulnerability assessment. *Sci. Rep.* **2014**, *4*, 6078. [CrossRef]

52. Alexandrakis, G.; Manasakis, C.; Kampanis, N.A. Valuating the effects of beach erosion to tourism revenue. A management perspective. *Ocean Coast. Manag.* **2015**, *111*, 1–11. [CrossRef]

53. Pardo-Pascual, J.; Almonacid-Caballer, J.; Ruiz, L.; Palomar-Vázquez, J. Automatic extraction of shorelines from Landsat TM and ETM+ multi-temporal images with subpixel precision. *Remote Sens. Environ.* **2012**, *123*, 1–11. [CrossRef]

54. Cenci, L.; Disperati, L.; Persichillo, P.; Oliveira, E.; Alves, F.; Phillips, M. Integrating remote sensing and GIS techniques for monitoring and modeling shoreline evolution to support coastal risk management. *Giscience Remote Sens.* **2017**, 1–21. [CrossRef]

55. Louati, M.; Saïdi, H.; Zargouni, F. Shoreline change assessment using remote sensing and GIS techniques: A case study of the Medjerda delta coast, Tunisia. *Arab. J. Geosci.* **2015**, *8*, 4239–4255. [CrossRef]

56. Liu, Q.; Trinder, J.; Turner, I. Automatic super-resolution shoreline change monitoring using Landsat archival data: A case study at Narrabeen-Collaroy Beach, Australia. *J. Appl. Remote Sens.* **2017**, *11*, 016036. [CrossRef]

57. Apostolopoulos, D.; Nikolakopoulos, K. Assessment and Quantification of the Accuracy of Low-and High-Resolution Remote Sensing Data for Shoreline Monitoring. *ISPRS Int. J. Geo-Inf.* **2020**, *9*, 391. [CrossRef]

58. Apostolopoulos, D.; Nikolakopoulos, K.; Boumpoulis, V.; Depountis, N. GIS based analysis and accuracy assessment of low-resolution satellite imagery for coastline monitoring. In *Proccedings of the SPIE 11534, Earth Resources and Environmental Remote Sensing/GIS Applications XI*; SPIE: Bellingham, WA, USA, 2020; Volume 115340B. [CrossRef]

59. Apostolopoulos, D.; Nikolakopoulos, K. A review and meta-analysis of Remote Sensing data, GIS methods, materials and indices used for monitoring the coastline evolution over the last twenty years. *Eur. J. Remote Sens.* **2021**. [CrossRef]

60. Almonacid-Caballer, J.; Sánchez-García, E.; Pardo-Pascual, J.E.; Balaguer-Beser, A.A.; Palomar-Vázquez, J. Evaluation of annual mean shoreline position deduced from Landsat imagery as a mid-term coastal evolution indicator. *Mar. Geol.* **2016**, *372*, 79–88. [CrossRef]

61. Aiello, A.; Canora, F.; Pasquariello, G.; Spilotro, G. Shoreline variations and coastal dynamics: A space–time data analysis of the Jonian littoral, Italy. *Estuar. Coast. Shelf Sci.* **2013**, *129*, 124–135. [CrossRef]

62. Ford, M. Shoreline changes interpreted from multi-temporal aerial photographs and high resolution satellite images: Wotje Atoll, Marshall Islands. *Remote Sens. Environ.* **2013**, *135*, 130–140. [CrossRef]

63. Kermani, S.; Boutiba, M.; Guendouz, M.; Guettouche, M.S.; Khelfani, D. Detection and analysis of shoreline changes using geospatial tools and automatic computation: Case of jijelian sandy coast (East Algeria). *Ocean Coast. Manag.* **2016**, *132*, 46–58. [CrossRef]

64. Bruno, M.F.; Molfetta, M.G.; Pratola, L.; Mossa, M.; Nutricato, R.; Morea, A.; Nitti, D.O.; Chiaradia, M.T. A Combined Approach of Field Data and Earth Observation for Coastal Risk Assessment. *Sensors* **2019**, *19*, 1399. [CrossRef]

65. Martínez, C.; Contreras-López, M.; Winckler, P.; Hidalgo, H.; Godoy, E.; Agredano, R. Coastal erosion in central Chile: A new hazard? *Ocean Coast. Manag.* **2018**, *156*, 141–155. [CrossRef]

66. Nikolakopoulos, K.; Konstantinopoulos, D.; Depountis, N.; Kavoura, K.; Sabatakakis, N.; Fakiris, E.; Christodoulou, D.; Papatheodorou, G. Coastal monitoring activities in the frame of TRITON project. In *Proccedings of the SPIE 11156, Earth Resources and Environmental Remote Sensing/GIS Applications X*; SPIE: Bellingham, WA, USA, 2019.

67. Thieler, E.R.; Himmelstoss, E.A.; Zichichi, J.L.; Ergul, A. *The Digital Shoreline Analysis System (DSAS) Version 4.0-an ArcGIS Extension for Calculating Shoreline Change*; U.S. Geological Survey: Woods Hole, MA, USA, 2009.

68. Ferentinos, G.; Brooks, M.; Doutsos, T. Quaternary tectonics in the Gulf of Patras, western Greece. *J. Struct. Geol.* **1985**, *7*, 713–717. [CrossRef]

69. Chronis, G.; Piper, D.; Anagnostou, C. Late Quaternary evolution of the Gulf of Patras, Greece: Tectonism, deltaic sedimentation and sea-level change. *Mar. Geol.* **1991**, *97*, 191–209. [CrossRef]

70. Hettiarachchi, H.; Brown, T. Use of SPT Blow Counts to Estimate Shear Strength Properties of Soils: Energy Balance Approach. *J. Geotech. Geoenviron. Eng.* **2009**, *135*, 830–834. [CrossRef]

71. Anders, F.J.; Byrnes, M.R. Accuracy of shoreline change rates as determined from maps and aerial photographs. *Shore Beach* **1991**, *59*, 17–26.

72. Fletcher, C.; Rooney, J.; Barbee, M.; Lim, S.-C.; Richmond, B. Mapping shoreline change using digital orthophotogrammetry on Maui, Hawaii. *J. Coast. Res.* **2003**, *38*, 106–124.

73. Thieler, E.R.; Danforth, W.W. Historical shoreline mapping. Part 1: Improving techniques and reducing positioning errors. *J. Coast. Res.* **1994**, *10*, 549–563.

74. Ford, M. Shoreline Changes on an Urban Atoll in the Central Pacific Ocean: Majuro Atoll, Marshall Islands. *J. Coast. Res.* **2012**, *28*, 11–22. [CrossRef]

75. Himmelstoss, E.A.; Henderson, R.E.; Kratzmann, M.G.; Farris, A.S. *Digital Shoreline Analysis System (DSAS) Version 5.0 User Guide*; U.S. Geological Survey: Woods Hole, MA, USA, 2018; Open-File Report 2018–1179.

76. Antonioli, F.; De Falco, G.; Presti, V.; Moretti, L.; Scardino, G.; Anzidei, M.; Bonaldo, D.; Carniel, S.; Leoni, G.; Furlani, S.; et al. Relative Sea-Level Rise and Potential Submersion Risk for 2100 on 16 Coastal Plains of the Mediterranean Sea. *Water* **2020**, *12*, 2173. [CrossRef]

77. Galassi, G.; Spada, G. Sea-level rise in the Mediterranean Sea by 2050: Roles of terrestrial ice melt, steric effects and glacial isostatic adjustment. *Glob. Planet. Chang.* **2014**, *123*, 55–66. [CrossRef]

78. Lambeck, K. Sea-level change and shore-line evolution in Aegean Greece since Upper Palaeolithic time. *Antiquity* **1996**, *70*, 588–611. [CrossRef]

79. Coca-Domínguez, O.; Ricaurte-Villota, C. Validation of the Hazard and Vulnerability Analysis of Coastal Erosion in the Caribbean and Pacific Coast of Colombia. *J. Mar. Sci. Eng.* **2019**, *7*, 260. [CrossRef]

80. Gallina, V.; Torresan, S.; Zabeo, A.; Critto, A.; Glade, T.; Marcomini, A. A Multi-Risk Methodology for the Assessment of Climate Change Impacts in Coastal Zones. *Sustainability* **2020**, *12*, 3697. [CrossRef]

81. Rizzo, A.; Vandelli, V.; Buhagiar, G.; Micallef, S.; Soldati, M. Coastal Vulnerability Assessment along the North-Eastern Sector of Gozo Island (Malta, Mediterranean Sea). *Water* **2020**, *12*, 1405. [CrossRef]

82. Hoque, M.A.A.; Ahmed, N.; Pradhan, B.; Roy, S. Assessment of coastal vulnerability to multi-hazardous events using geospatial techniques along the eastern coast of Bangladesh. *Ocean Coast. Manag.* **2019**, *181*, 104898. [CrossRef]

83. Pantusa, D.; D'Alessandro, F.; Riefolo, L.; Principato, F.; Tomasicchio, G.R. Application of a coastal vulnerability index. A case study along the Apulian Coastline, Italy. *Water* **2018**, *10*, 1218. [CrossRef]

84. Perez, B.E.G.; Selvaraj, J.J. Evaluation of coastal vulnerability for the District of Buenaventura, Colombia: A geospatial approach. *Remote Sens. Appl. Soc. Environ.* **2019**, *16*, 100263. [CrossRef]

85. Sahana, M.; Hong, H.; Ahmed, R.; Patel, P.; Bhakat, P.; Sajjad, H. Assessing coastal island vulnerability in the Sundarban Biosphere Reserve, India, using geospatial technology. *Environ. Earth Sci.* **2019**, *78*, 304. [CrossRef]

86. Boruff, B.J.; Emrich, C.; Cutter, S.L. Erosion hazard vulnerability of US coastal counties. *J. Coast. Res.* **2005**, *21*, 932–942. [CrossRef]

87. Ozyurt, G.; Ergin, A.; Baykal, C. Coastal vulnerability assessment to sea level rise integrated with analytical hierarchy process. *Coast. Eng. Proc.* **2010**, *32*, 6. [CrossRef]

88. Bagdanavičiūtė, I.; Kelpšaitė, L.; Soomere, T. Multi-criteria evaluation approach to coastal vulnerability index development in micro-tidal low-lying areas. *Ocean Coast. Manag.* **2015**, *104*, 124–135. [CrossRef]

89. Díaz-Cuevas, P.; Prieto-Campos, A.; Ojeda-Zújar, J. Developing a beach erosion sensitivity indicator using relational spatial databases and Analytic Hierarchy Process. *Ocean Coast. Manag.* **2020**, *189*, 105146. [CrossRef]

90. Sekovski, I.; Del Río, L.; Armaroli, C. Development of a coastal vulnerability index using analytical hierarchy process and application to Ravenna province (Italy). *Ocean Coast. Manag.* **2020**, *183*, 104982. [CrossRef]

91. Hereher, M.; Al-Awadhi, T.; Al-Hatrushi, S.; Charabi, Y.; Mansour, S.; Al-Nasiri, N.; Sherief, Y.; El-Kenawy, A. Assessment of the coastal vulnerability to sea level rise: Sultanate of Oman. *Environ. Earth Sci.* **2020**, *79*, 369. [CrossRef]

92. Rizzo, A.; Aucelli, P.; Gracia, F.; Anfuso, G. A novelty coastal susceptibility assessment method: Application to Valdelagrana area (SW Spain). *J. Coast. Conserv.* **2018**, *22*, 973–987. [CrossRef]

93. Audere, M.; Robin, M. Assessment of the vulnerability of sandy coasts to erosion (short and medium term) for coastal risk mapping (Vendee, W France). *Ocean Coast. Manag.* **2021**, *201*, 105452. [CrossRef]

94. Zhang, Y.; Wu, W.; Arkema, K.; Han, B.; Lu, F.; Ruckelshaus, M.; Ouyang, Z. Coastal vulnerability to climate change in China's Bohai Economic Rim. *Environ. Int.* **2021**, *147*. [CrossRef]